Emerald International Journal of Numerical Methods for Heat and Fluid Flow

High-Rayleigh heat transfer flow: thermal stratification analysis and assessment of Boussinesq approach

Journal:	*International Journal of Numerical Methods for Heat and Fluid Flow*
Manuscript ID	HFF-05-2016-0176.R1
Manuscript Type:	Research Article
Keywords:	CFD, Heat Transfer, Boussinesq, High Rayleigh flow

HIGH-RAYLEIGH HEAT TRANSFER FLOW: THERMAL STRATIFICATION ANALYSIS AND ASSESSMENT OF BOUSSINESQ APPROACH

Santiago F. Corzo[a], Damian E. Ramajo[a] and Norberto M. Nigro[a]

[a]*Research center for Computational Methods CIMEC-UNL-CONICET, Colectora ruta 168, km 472, paraje el pozo (3000) Santa Fe, Argentina, (+54-342-4511594), santiagofcorzo@gmail.com, http://www.cimec.org.ar/twiki/bin/view/Cimec/*

Keywords: CFD, Heat Transfer, Boussinesq approach, High Rayleigh flow

Abstract. Natural convection heat transfer associated to fluid-dynamics phenomena has been extensively studied by means of experimental and numerical techniques in many scientific and industrial-related applications. High Rayleigh number (*Ra*) regimes are particularly challenging to be simulated in three-dimensional domains due to flow instability and the influence of turbulence models among others. Despite the efforts devoted to study these phenomena, the literature data remains scarce. Evidence shows that the Boussinesq approach, with constant thermal expansion coefficient, induces a body force that is linearly depending on the temperature. Therefore, the magnitude of the buoyancy force affects equally both cold and hot walls, leading to perfectly antisymmetric solutions. On the other hand, for high *Ra* problems commonly found in liquid systems, compressible solvers allow introducing more realistic constitutive relationships for the density and the other properties. As a result of that, the buoyancy effect at the cold and hot walls becomes different, especially during the transient stage of the simulation. This induces transient heat imbalances leading to fluid averaged temperatures higher than the obtained from Boussinesq. Consequently, the wall heat transfer is not the same as the that obtained from the Boussinesq solution. In this paper the Boussinesq approach is assessed for a wide range of *Ra* ($10^6 < \mathrm{Ra} < 10^{12}$) in two-dimensional (square cavity) and three-dimensional air and liquid-filled problems. The range of suitability of this approach was evaluated by comparing with the available experimental data and numerical results from a compressible solver. Moreover, the thermal and flow patterns and the stratification parameter *S* as well as the wall heat transfer were quantified while obtaining a correlation between *Ra* and *S*, which is useful to characterize the thermal pattern.

LIST OF SYMBOLS

p: Pressure.
$p_{rgh} = p - \rho \mathbf{g} \cdot \mathbf{x}$: Dynamic pressure.
t: Time.
$\mathbf{u}$: Velocity.
$\mathbf{x}$: Spatial coordinate.
h: Enthalpy.
$U = \frac{\mathbf{u}}{u_{NC}}$: Horizontal dimensionless velocity.
$V = \frac{\mathbf{v}}{u_{NC}}$: Vertical dimensionless velocity.
$u_{NC} = \frac{\alpha}{L} Ra^{1/2}$: Natural convection characteristic velocity.
$X = \frac{x}{L}$: Horizontal dimensionless coordinate.
$Y = \frac{y}{L}$: Vertical dimensionless coordinate.
$Pr = \frac{\nu}{\alpha}$: Prandtl number.
h: Convective heat transfer coefficient.
ν: Kinematic viscosity.
μ: Dynamic viscosity.
α: Thermal diffusivity.
T: Temperature.
T_h: Hot-wall temperature.
T_c: Cold-wall temperature.
T_{avr}: Fluid average temperature.
$T_{mw} = \frac{T_h + T_c}{2}$: Mean temperature between the hot and cold walls.
$T_{\mathtt{diff}} = T_{avr} - T_{mw}$: Difference of temperature from the mean temperature calculated and the expected from the Boussinesq approach.
$\varepsilon_{\Delta T} = 100 \frac{T_{\mathtt{diff}}}{\Delta T}$: Relative error of Boussinesq approach.
ΔT: temperature range of the problem. Typically assumed as $T_h - T_c$ in differentially heat cavities.
ρ: Density.

$\theta = \frac{T - T_c}{T_h - T_c}$: Dimensionless temperature.
$\theta_{limit} = \frac{T_h - T_c}{T_c}$: validity criterion of the Boussinesq approach according Zhong, Yang and Lloyd.
L: characteristic length.
$Ra = \frac{g\beta L^3 (T_h - T_c)}{\alpha \nu}$: Rayleigh number.
$\mathbf{g}$: Gravity acceleration.
β: Thermal expansion coefficient.
$\tau_{\mathbf{ij}}$: Molecular stress tensor.
$\tau_{\mathbf{ij,t}}$: Turbulent stress tensor.
δ_{ij}: Dirac tensor.
k: Turbulent kinetic energy.
$R_{ij}{}^{D}$: Deviatoric Reynolds stress tensor.
V: Volume.
Δ: Filter length scale.
$C_S = 0.2$: Smagorinsky constant (0.2 by default).
$|\mathbf{S}|$: Magnitude of the resolved strain rate tensor.
Δ_{mesh}: Cell volume.
$\kappa' = 0.4187$: Von Kármán constant.

$C_\Delta = 0.158$: Van Driest constant.
$A^+ = 26$: Constant for turbulent model.
$y^+ = yu_\tau/\nu$: Dimensionless distance from the wall.
$u_\tau = (\tau_w/\rho)^{1/2}$: Near-wall friction velocity.
τ_w: Wall shear stress.
$S = \frac{\partial \theta}{\partial x}$: Stratification parameter.
P: Cell of the grid.
P: Heat power.
δ_f: Flow layer thickness.
δ_t: Thermal layer thickness.
A_h: Height aspect ratio.
A_d: Depth aspect ratio.
q: Wall heat flux.
$\varepsilon_r = \left| \frac{\rho_{est} - \rho}{(\rho - \rho_{mw})_{exact}} \right|$: Density error.

LIST OF SUBINDEX

0: Reference value.
t: Turbulent.
eff: Effective value (laminar + turbulent contributions).
c: Cold temperature side.
h: Hot temperature side.

LIST OF ACRONYMS

CFD: Computational fluid dynamics.
DHC: Differentially Heated Cavities.
FVM: Finite Volume Method.
CV: Control Volume.
LES: Large eddy Simulation.

1 INTRODUCTION

Natural convection heat transfer in closed domains is of great importance in many engineering applications such as ventilation of rooms, heat exchangers, boilers, nuclear reactors and energy storage devices. It has been largely studied in the past with the help of experimental data, although limited to simple geometries and particularly in the so-called 'Differentially Heated Cavities' (DHC), which are one of the most classical benchmarks in heat transfer (Ampofo and Karayiannis, 2003) (De Vahl Davis, 1983)(Aydin and Yang, 2000) (Rasoul and Prinos, 1997). Although DHC configuration represents a very simple geometry, the flow complexity arrives from the strong coupling between the continuity and thermal equations for sufficiently high *Ra* (Barhaghi and Davidson, 2007). Therefore, *DHC* is often used for assessing numerical algorithms (Le Quéré, 1991). Since the last decade, Computational Fluid Dynamics (CFD) has evolved to become a valuable tool for analyzing single-phase flows in geometries with higher complexity than *DHC*. Even though CFD is currently employed both for design and safety assessment of operating equipments, early numerical studies were carried out using very simple geometries as in De Vahl Davis et al. (De Vahl Davis, 1983), who solved 2D configurations for low *Ra* ($10^3 < Ra < 10^6$) laminar flow. Later, numerical and experimental works (Patterson and Imberger, 1980) (Salat et al., 2004) (Navamani and Murugan, 2010) addressed this phenomenon for higher *Ra*, but almost exclusively in air-filled cavities. On the other hand, if the working fluid is water, obtaining solutions for the governing equations becomes more complicated, as the boundary layer becomes thinner than for air at the same conditions (Kizildag et al., 2011). These main previous studies covered laminar and low turbulence flows focusing on three aspects to know:

- The critical Rayleigh number Ra_{crit} for the transition to unsteadiness (until flow becomes time-dependent)
- The transition Rayleigh number Ra_{tran} for which the flow changes from 2D to 3D
- The thermal stratification parameter (S).

The key question to answer was whether the transitions to unsteadiness and three dimensionality are simultaneous or otherwise there is a range of *Ra* for which the flow is unsteady but still 2D. This question was addressed by Henkes et al. (Henkes and Le Quéré, 1996) for a cubic cavity of height aspect ratio $A_h = 1$ and depth aspect ratio $A_d = 0.1$. It was observed that the most significant difference between 2D and 3D flows is an increase of the heat transfer coefficient in the 3D cases. Later, Trias et al. (Trias et al., 2007) found that for high *Ra* there are significant differences in the flow dynamics between 2D and 3D. Large unsteady eddies observed in 2D simulations did not persist in the 3D counterparts because the vortex energy is rapidly transferred down to smaller scales causing a reduction of the large-scale mixing effects. As a consequence, the stratified cavity core remains motionless. They also concluded that for the turbulent regime the 3D simulations are necessary to get an accurate description of the flow. More recently, Trias et al.(Trias et al., 2010) numerically demonstrated that in a general *DHC* problem, with periodic vertical boundary conditions, the flow is not forced to be 3D and consequently, three different flows can be found: 2D steady, 2D unsteady and 3D unsteady. Summarizing, the critical Ra_{crit} and the transition Ra_{tran} are not necessarily the same although they are closer to each other.

Another important conclusion from the point of view of the engineering applications is that the flow behavior is strongly dependent on the height cavity aspect ratio A_h, e.g., for a square

cavity ($A_h = 1$) with adiabatic horizontal walls, Le Quéré et al. (Le Quéré and Behnia, 1998) identified the critical number as $Ra_{crit} = 1.82 \times 10^8$. Moreover, they studied the occurrence of time-dependent chaotic flows at $Ra = 10^{10}$. Regarding the stratification S, it perhaps is the only one parameter to quantify the degree of non-homogeneity of the temperature pattern. In this sense, Trias et al.(Trias et al., 2010) provided information for a wide range of Ra from $Ra = 6.4 \times 10^6$ up to 10^{11} in a slim air-filled cavity ($A_h = 4$) finding that stratification is $S = 1.25$ for $Ra = 3 \times 10^{10}$ whereas it rises to $S = 1.41$ for the highest Ra.

The *DHC* has been a useful data resource to develop and assess CFD codes, which are used daily in the study of thermal industrial devises such as powerful electric transformers or heat exchangers. These simulations are normally accomplished through incompressible solvers, which use the Boussinesq approach. This is a very simplistic model, which consists of the following: density is assumed constant except when it directly induces buoyant forces, all other fluid properties are assumed constant and viscous dissipation is assumed negligible (Gray and Giorgini, 1976). It is invariably able to perform simulations within a much shorter computational time span. On the contrary, a variable-properties model estimates all the fluid properties as a function of the local temperature and pressure at every time step, thereby imposing substantial computational resource requirements and also reducing convergence. That is probably the main reason behind the popularity of Boussinesq approach (Krishnani and Basu, 2016). In this approach the buoyant force has a linear dependency with temperature, easily achieved by applying a thermal expansion coefficient β calculated for a mean temperature (T_{mw}).Boussinesq approach is frequently employed due to its simplicity and stability in theoretical natural convection calculations (Zhong et al., 1985) but also in industrial applications (Basit et al., 2007), (Zvirin, 1982), (Jiang et al., 2002). However, it is known that it is only accurate for low and medium Ra flows, low β or when temperature variation is bounded in a narrow range. As already mentioned, several studies (Becker and Braack, 2002) (Vierendeels et al., 2004) (Darbandi and Hosseinizadeh, 2006) addressed natural convection for low and medium Ra in air or gas systems providing numerical results for *DHC* using compressible models.

Other works additionally compare the Boussinesq approach with compressible models that use the ideal gas law (Hung and Cheng, 2002)(Mlaouah et al., 1997) (Kumar and Eswaran, 2010). Nevertheless, only a few have been undertaken to discuss the limitations of the Boussinesq approach (Barhaghi and Davidson, 2007) (Pesso and Piva, 2009), although adopting the limit criterion from Gray et al. (Gray and Giorgini, 1976), which were one of the first in to establish a limit for the validity of Boussinesq approach. Gray et al. used a level approach technique of the Navier-Stokes equations by introducing linear approximations for all the fluid properties before applying a non-dimensionalization operation over the equations. Then, they introduced a limit criteria to bound the properties variation by assuming certain restrictions for which the compressible Navier-Stokes equations become similar to the incompressible Boussinesq form. They found that to fulfill this procedure the variation of the fluid properties with respect to a reference value (ρ/ρ_0, Cp/Cp_0, μ/μ_0, α/α_0, κ/κ_0) must be limited up to 10%. This accomplishment introduces several restrictions in terms of the characteristic length (L), the temperature variation and the Ra (e.g., for air this criterion limits the temperature variation range to $28.6°C$). Of course, these criterion limits become more restrictive for liquids. A much lower restriction was reached by Zhong et al. (Zhong et al., 1985), who defined a variable $\theta_{limit} = \frac{T_h - T_c}{T_c}$ and found that even for $\theta_{limit} = 0.2$ and $Ra = 10^6$ the Boussinesq approach still predicts the correct Nusselt number within 2%, even though the vertical velocity components may be overestimated by as much as 20%. The authors go farther indicating that the θ_{limit} for which Boussinesq is able to predict heat transfer within a 5% accuracy is given for the fol-

lowing expression: $\theta_{limit} = 0.0244Ra^{0.243}$. Unfortunately, this broad criterion was formulated for low and medium Ra. For example, $\theta_{limit}(Ra = 10^4) = 0.22$, $\theta_{limit}(Ra = 10^5) = 0.4$ and $\theta_{limit}(Ra = 10^6) = 0.7$.

The criterion from Gray et al. has different interpretations. Mlaouah et al.(Mlaouah et al., 1997) defined that Boussinesq can be accurately applied when the ratio between the density variation range and the mean density (at T_{mw}) is less than 0.1 ($\frac{\rho_{max}-\rho_{min}}{\rho_0} < 0.1$). Although the majority of the studies adopt fluid properties calculated for the mean temperature ($T_0 = T_{mw}$), the study of Zhong et al. (Zhong et al., 1985) showed that more accurate solutions are found when the fluid properties are calculated for a temperature closer to the lower limit ($T_0 = T_c + 0.25(T_h - T_c)$).

Whichever the criterion, typical industrial processes work in a wide temperature range (e.g., T_h - $T_c > 60°C$). Therefore, the density changes are farther to be linear and symmetric with respect to T_{mw}. Consequently, this general criterion seems inappropriate because it considers the density variation but it ignores how the density changes ($\frac{\partial \rho}{\partial T}$). Instead, a more general criterion should be based on the difference between the true density and the linearly estimated from Boussinesq for the limit range of temperatures T_c and T_h. Of course, in many heater systems the boundary condition is a heat flux and the temperature limits are not always known a priori.

Throughout the years the Boussinesq approach has been widely employed without concern about its validity. However, several authors have demonstrated that, even without fulfilling the aforementioned criterion, the Boussinesq approach is in good agreement with experimental data for low to high Ra problems. At high Ra, the 3D simulations from Le Quéré (Le Quéré, 1991) ($Ra = 10^7$ and 10^8) are the widely known references. These cases were numerically reproduced by the authors in a previous research (Corzo et al., 2011) showing the suitability of the Boussinesq approach for modeling these Ra regimes. On the other hand, literature data regarding very high Ra benchmarks is still scarce. The DHC tests defined by Tian et al.(Tian and Karayiannis, 2000) and Ampofo et al. (Ampofo and Karayiannis, 2003) ($Ra = 1.59 \times 10^9$) employing an air-filled cavity overcome the limit ($\Delta T = 40°C$). Nevertheless, accurate solutions for velocity and temperature pattern and heat transfer were obtained by Peng et al.(Peng and Davidson, 2000) and also by the current study. Another example is from Barhaghi et al. (Barhaghi et al., 2006) who compared numerical results with experimental test developed by Tsuji et al. (Tsuji and Nagano, 1988) for a concentric vertical shell with a central hot-rod ($\Delta T = 80°C$). Despite the large temperature range, they found very good agreement with experimental data. Other contribution from the same authors was reported in 2007 (Barhaghi and Davidson, 2007). In this case they studied the behavior of air flowing between two vertical walls and heated through one of this by a constant heat flux. Although the temperature difference between the hot wall and the entering air increased more than $100°C$, the numerical results based on Boussinesq approach were in good accordance with the measured data.

It should be noted that in very simple geometries (such as DHC) the Boussinesq approach leads to a solution where the averaged temperature of the fluid is exactly the mean temperature between the hot and cold walls ($T_{avr} = T_{mw} = (T_c + T_h)/2$). Furthermore, the time-averaged solutions are quite antisymmetric concerning the mid-planes and the convective heat transfer coefficient h is the same for the cold and hot walls. In fact, the thermal expansion coefficient β is far from being constant along the wide range of operating temperatures (from T_c to T_h). Consequently, it must be expected that buoyancy forces differ at the hot and cold sides, thus leading to different near-wall velocities. Although these differences can be small, they should not be negligible, thus inducing a little more heat flux in one of the walls until the system reach

steady-state conditions. Therefore, the averaged temperature T_{avr} becomes a slightly higher than the estimated from Boussinesq ($T_{avr} > T_{mw}$). This characteristic difference was found by Kizildag et al. (Kizildag et al., 2011) although without giving enough significance. On the contrary, in the current work this behavior is studied in deep for a large range of operation temperatures and it is considered as the basis for a new criterion limit for the validity of the Boussinesq approach.

Nonetheless the efforts done in academic cases, it is still insufficient to deeply understand the behavior of high-performance industrial systems, which typically operate under very high *Ra* and turbulent regimes, employing liquids instead of gases because of the higher heat capacity of the former. For these fluids, the *Pr* can be higher than 5 and the *Ra* easily increases up to 10^{11} due to the wide temperature ranges and the characteristic lengths of the devices. In this scenario, engineers and designers undergo the lack of experimental data and knowledge. Therefore, there are a few numerical studies in which the Boussinesq approach is assessed against non-Boussinesq solvers. Krishnani et al.(Krishnani and Basu, 2016) used Boussinesq for studying the nonlinear stability of a 3D water natural circulating loop concluding that the approach is not valid because it over predicts the steady-state mass flow and consequently, it predicts instability for much lower power levels. On the other hand, Kizildag et al. (Kizildag et al., 2011) performed 2D comparisons taking special care of the grid resolution finding good agreement in the heat transfer but also significant differences in the near wall velocity profiles, which are similar to that found for Zhong et al. (Zhong et al., 1985). It should be noted that in both cases the criteria limits from Gray was not fulfilled. In contrast with the significant differences in the velocity profiles found by Kizildag et al. and Zhong et al. in 2D domains, an acceptable accordance was found by Barhaghi et al. (Barhaghi and Davidson, 2007) and the numerical data here reported.

The present work deals with air-filled and water-filled cavity problems ranging from low (10^3) to very high (4.1×10^{11}) Rayleigh. Regarding the very higher *Ra*, simulations were performed both with the Boussinesq approach (constant properties) and with a variable-properties solver. For the latter, suitable correlations were obtained from the high temperature-pressure database IAPWS-F95 (Wagner and Pruß, 2002). Comparison allows determining the validity of the incompressible approach for solving high *Ra* industrial problems. The relationship between the *Ra*, the thermal patterns and the stratification parameter *S* was also studied.

Summarizing, the current work addressees the following topics:

- Boussinesq approach vs. variable-properties formulation.
- Two-dimensional vs. three-dimensional models.
- Transient wall heat flux and steady-state average temperature.
- Temperature patterns and thermal stratification.

2 MATHEMATICAL FORMULATION AND COMPUTATIONAL METHODS

The more relevant parameters to characterize the intensity of the buoyant motion and the heat transfer in natural convection systems are the dimensionless Rayleigh (*Ra*) and Nusselt (*Nu*) numbers defined as:

$$Ra = \frac{g\beta L^3 (T_h - T_c)}{\alpha \nu} \tag{1}$$

$$Nu = \frac{hL}{\kappa} = \frac{q_w}{(T_w - T_{avr})}\frac{L}{\kappa} = \frac{\kappa_{eff}\nabla T}{(T_w - T_{avr})}\frac{L}{\kappa} \tag{2}$$

where L is the characteristic size (typically the height) and $(T_h - T_c)$ is the largest temperature difference, β is the thermal expansion coefficient, g is the acceleration due to gravity, α is the thermal diffusivity, ν is the kinematic viscosity, T_{avr} is the fluid average temperature and $\kappa_{eff} = \alpha_{eff}\rho Cp$ is the effective conductivity, which includes the molecular conductivity and turbulence effects.

The mathematical background presented below is based on the solvers `buoyantBoussinesqPimpleFoam` and `buoyantPimpleFoam` for incompressible and compressible formulations, respectively. These solvers are currently implemented in OpenFOAM 2.3.1 (Open Field Operation and Manipulation), which is a free and open source toolbox package released under the GNU General Public License, widely used in the scientific and industrial communities all around the world. It has parallel computing capabilities, which become suitable for simulating engineering as well as academic problems such as those considered in this work.

2.1 Incompressible formulation

As stated above, in natural convection problems the driven force is given by changes in the fluid density due to local temperature variations, but under certain conditions the thermodynamic properties can be assumed to be constant by adding an explicit buoyancy body force term in the momentum equation. This is usually achieved by means of the Boussinesq approximation, coupling the energy and the momentum equations.

The governing equations for Newtonian incompressible flow are presented in Equations 3 to 14. The continuity equation takes the following form:

$$\frac{\partial u_j}{\partial x_j} = 0 \tag{3}$$

The momentum equation is written as:

$$\frac{\partial u_j}{\partial t} + \frac{\partial u_j u_i}{\partial x_j} = -\frac{1}{\rho_0}\frac{\partial p}{\partial x_i} + \frac{1}{\rho_0}\frac{\partial}{\partial x_j}(\tau_{ij} + \tau_{t,ij}) + \frac{\rho}{\rho_0}g_i \tag{4}$$

where the sub-index 0 indicates that the thermodynamics properties are calculated for a reference temperature (T_0). For DHC problems, T_0 is typically calculated for the mean temperature among the walls. τ_{ij} and $\tau_{t,ij}$ are the laminar and turbulent stress tensors, respectively. τ_{ij} is given by the following expression:

$$\tau_{ij} = \mu\left[\left(\frac{\partial u_i}{\partial x_j} + \frac{\partial u_j}{\partial x_i}\right) - \frac{2}{3}\left(\frac{\partial u_k}{\partial x_k}\right)\delta_{ij}\right] \tag{5}$$

In Equation 5, μ is the molecular viscosity and δ_{ij} is the Dirac tensor. Replacing μ with a constant reference value ($\mu = \mu_0$) in Equation 5 and then replacing it into the momentum equation ($UEqn$) 4 leads to:

$$\frac{\partial u_j}{\partial t} + \frac{\partial (u_j u_i)}{\partial x_j} = -\frac{\partial}{\partial x_i}\left(\frac{p}{\rho_0} + \frac{2}{3}k\right)$$
$$+\frac{\partial}{\partial x_j}\left\{\nu_0\left[\left(\frac{\partial u_i}{\partial x_j} + \frac{\partial u_j}{\partial x_i}\right) - \frac{2}{3}\left(\frac{\partial u_k}{\partial x_k}\right)\delta_{ij}\right] - R^D_{ij}\right\}$$

$$+g_i\left(1+\frac{\rho-\rho_0}{\rho_0}\right) \tag{6}$$

where $\nu_0=\mu_0/\rho_0$, k is the kinetic energy and R_{ij}^D is the deviatoric part of the Reynolds stress tensor. The last term in the right hand side is the buoyancy term, which is accomplished by the Boussinesq approximation in the next statement. It leads to the following $UEqn$:

$$\frac{\partial u_j}{\partial t}+\frac{\partial(u_j u_i)}{\partial x_j}=-\frac{\partial}{\partial x_i}\left(\frac{p}{\rho_0}+\frac{2}{3}k\right)$$
$$+\frac{\partial}{\partial x_j}\left\{\nu_{eff}\left[\left(\frac{\partial u_i}{\partial x_j}+\frac{\partial u_j}{\partial x_i}\right)-\frac{2}{3}\left(\frac{\partial u_k}{\partial x_k}\right)\delta_{ij}\right]\right\}$$
$$+g_i\left[1-\beta(T-T_0)\right] \tag{7}$$

where $\nu_{eff}=\nu_0+\nu_t$ is the effective kinematic viscosity and β is the volumetric thermal expansion coefficient.An average constant value for β can be estimated as:

$$\beta=\frac{1}{v}\frac{\partial v}{\partial T}=\rho\frac{\partial}{\partial T}\frac{1}{\rho}\longrightarrow\beta_0=\rho_0\frac{\Delta\left(\frac{1}{\rho}\right)}{\Delta T}=\left(\frac{\rho_h+\rho_c}{2}\right)\frac{\frac{1}{\rho_h}-\frac{1}{\rho_c}}{T_h-T_c} \tag{8}$$

Assuming that for incompressible flow the density is constant, the continuity equation becomes a constraint for the velocity field (see Equation 3). In mathematical terms, pressure works as a Lagrange multiplier over the velocity field space restricted to only divergence free solutions. Despite the fact that there is no explicit expression for the pressure derived from the constitutive equations, it can be obtained by applying the divergence operator to the momentum equation. Thus, the Poisson equation is obtained.

The set of governing equations is completed with the energy balance equation ($EEqn$), formulated in terms of temperature instead of entalphy:

$$\frac{\partial T}{\partial t}+\frac{\partial}{\partial x_j}(Tu_j)=\frac{\partial}{\partial x_k}\left(\alpha_{eff}\frac{\partial T}{\partial x_k}\right) \tag{9}$$

where α_{eff} is the effective thermal diffusivity, which accounts for the molecular and turbulent diffusion:

$$\alpha_{eff}=\frac{\nu_0}{Pr}+\frac{\nu_t}{Pr_t} \tag{10}$$

In Equation 10, Pr is the Prandtl number ($Pr=Cp\mu_0/\kappa$) and Pr_t is the turbulent Prandtl number ($Pr_t=Cp\mu_t/\kappa_t$), which is assumed to have a constant value of 0.7.

2.2 Compressible formulation

As it was mentioned previously, the Boussinesq approximation would not be a appropriated option to solve buoyancy driven problems under certain conditions. In these situations, the compressible formulation incorporating a density law seems to be the more suitable choice. Based on the IAPWS-F95 database, appropriated correlations $f(T,p)$ for water density (ρ), viscosity (μ) and heat capacity (Cp) were made for the range of temperatures and pressures simulated.

The compressible continuity equation takes the following form:

$$\frac{\partial \rho}{\partial t} + \frac{\partial (\rho u_j)}{\partial x_j} = 0 \tag{11}$$

The momentum ($UEqn$) is written as:

$$\frac{\partial (\rho u_j)}{\partial t} + \frac{\partial (\rho u_j u_i)}{\partial x_j} = -\frac{\partial p}{\partial x_i} + \frac{\partial}{\partial x_j}(\tau_{ij} + \tau_{t,ij}) + \rho g_i \tag{12}$$

Subtracting the hydrostatic pressure $p_{rgh} = p - \rho \mathbf{g}\mathbf{x}$, the equation 12 takes the follows form:

$$\frac{\partial (\rho u_j)}{\partial t} + \frac{\partial (\rho u_j u_i)}{\partial x_j} = -\frac{\partial p_{rgh}}{\partial x_i} + \frac{\partial}{\partial x_j}(\tau_{ij} + \tau_{t,ij}) - g_i x \frac{\partial \rho}{\partial x_i} \tag{13}$$

Finally, the energy equation ($EEqn$) is written in conservative form in terms of enthalpy:

$$\frac{\partial (\rho h)}{\partial t} + \frac{\partial}{\partial x_j}(\rho h u_j) - \frac{\partial p}{\partial t} = \frac{\partial}{\partial x_k}\left(\kappa_{eff} \frac{\partial T}{\partial x_k}\right) \tag{14}$$

2.3 Turbulence models

Both for the compressible and incompressible solvers the turbulent closure equation is obtained from the Static Smagorinsky Large Eddy Simulation (LES) model (Smagorinsky, 1963), in which the subgrid-scale eddy viscosity ν_t is defined as:

$$\nu_t = C_S^2 \Delta^2 |\mathbf{S}| \tag{15}$$

where C_S is the Smagorinsky constant ($C_S \approx 0.2$) and Δ is the filter length scale. $|\mathbf{S}|$ is the magnitude of the resolved strain rate tensor. Ferziger et al. (Ferziger and Peric, 2002) suggested that turbulence must be properly damped close to the walls. Therefore, in this study the well known Van Driest function (Van Driest, 2012) was selected to modify the filter length scale as follow:

$$\Delta = \min\left(\Delta_{mesh}^{1/3}, \frac{\kappa'}{C_\Delta}\right)\left(1 - e^{-y^+/A^+}\right) \tag{16}$$

where Δ_{mesh} is the cell volume, $\kappa' = 0.4187$ is the von Kármán constant and $C_\Delta = 0.158$. y^+ is a dimensional distance ($y^+ = y u_\tau / \nu$) computed from the real distance from the wall (y) and the near-wall friction velocity (u_τ). $u_\tau = (\tau_w/\rho)^{1/2}$ is obtained from the wall shear stress (τ_w). The constant A^+ usually takes the value of 26. This modified filter length scale Δ damps the turbulence viscosity near the walls, where turbulence should be negligible if sufficiently finer meshes are employed.

2.4 Numerical implementation

The governing equations presented above form a partial differential system equation, which can be transformed to an algebraic system by applying spatial and temporal discretization. This is accomplished in OpenFOAM by Finite Volume Method (FVM) (Versteeg and Malalasekera, 2007). In FVM each Control Volume (CV) has a centroid (P) bounded by a set of faces (f). Each face is shared by two CVs for internal faces while that for boundary faces these belong to only one CV. The cells surrounding P are called neighbors (N). The FVM requires that the

governing equations be spatially satisfied in an integral form in each CV. For time integration, the equations are rewritten by the backward Euler formulation.

The integral form of the incompressible $UEqn$ (Eqn. 7) takes the following expression:

$$\frac{V_\mathrm{P}}{\Delta t}(\mathbf{u}^n - \mathbf{u}^{n-1}) + \sum_f (\mathbf{u}^{n-1})_f \cdot \mathbf{S_f}\mathbf{u}^n = -\frac{1}{\rho_0}\sum_f p_f \cdot \mathbf{S_f} + \frac{1}{\rho_0}\sum_f (\tau + \tau_\mathbf{t})_f \cdot \mathbf{S_f} + \mathbf{g}\left[1 - \beta(T - T_0)\right] V_\mathrm{P} \tag{17}$$

As noted, the CV is bounded by faces (f) and the term inside the divergence operator is transformed into a summatory of integrals over the faces by applying the Gauss theorem. Similarly, the compressible $UEqn$ (Eqn. 12) is written as:

$$\frac{V_\mathrm{P}}{\Delta t}(\rho^n\mathbf{u}^n - \rho^{n-1}\mathbf{u}^{n-1}) + \sum_f (\rho^{n-1}\mathbf{u}^{n-1})_f \cdot \mathbf{S_f}\mathbf{u}^n = -\sum_f (p_{rgh})_f \cdot \mathbf{S_f} + \sum_f (\tau + \tau_\mathbf{t})_f \cdot \mathbf{S_f} - \mathbf{g}\mathbf{x}\sum_f \rho_f \cdot \mathbf{S_f} \tag{18}$$

In both solvers the convective term in the $UEqn$ has a quadratic non-linear dependence with the velocity, which could affect the stability of the solutions. There are two possible solutions for this problem; either to use a non-linear system solver or to linearise this term (Ferziger and Peric, 2002). The latter option is achieved in OpenFOAM by using the volumetric or the mass fluxes from the previous time step ($F^{n-1} = (\mathbf{u}^{n-1})_f \cdot \mathbf{S_f}$ and $F^{n-1} = (\rho^{n-1}\mathbf{u}^{n-1})_f \cdot \mathbf{S_f}$ for the incompressible and compressible formulation respectively). Thus, the incompressible $UEqn$ becomes:

$$\left[a_\mathrm{P} {u_\mathrm{P}}^n + \sum a_N {u_N}^n\right] = (RHS)_\mathrm{P} + \left(-\frac{1}{\rho_0}\sum_f (p^n)_f S_f + V_\mathrm{P}\frac{\rho}{\rho_0}g\right)_{pEqn} \tag{19}$$

and the compressible $UEqn$ takes the following form:

$$\left[a_\mathrm{P} {u_\mathrm{P}}^n + \sum a_N {u_N}^n\right] = (RHS)_\mathrm{P} + \left(\sum_f (p^n_{rgh})_f S_f + \mathbf{g}\mathbf{x}\sum_f \rho_f \cdot S_f\right)_{pEqn} \tag{20}$$

where a_P are the diagonal values of cell P, a_N are the off-diagonal values and $(RHS)_\mathrm{P}$ is the right hand side of the $UEqn$. Finally, for the incompressible and compressible solvers the velocity can be computed from the linear momentum equations 19 or 20 as:

$$u_\mathrm{P} = \frac{1}{a_\mathrm{P}}\left[H(\mathbf{u}) + \left(-\frac{1}{\rho_0}\sum_f (p^n)_f S_f + V_\mathrm{P}\frac{\rho}{\rho_0}g\right)_{pEqn}\right] \tag{21}$$

$$u_\mathrm{P} = \frac{1}{a_\mathrm{P}}\left[H(\mathbf{u}) + \left(-\sum_f ({p_{rgh}}^n)_f S_f + \mathbf{g_i}x\sum_f (\rho^n)_f S_f\right)_{pEqn}\right] \tag{22}$$

The $H(u)$ operator in Equations 21 and 22 is the RHS minus the off-diagonal values multiplied by the unknown velocity vector.

$$H(u) = (RHS)_\mathrm{P} - \sum a_N {u_N}^n \tag{23}$$

Since no pressure equation is given, it is necessary to devise an strategy to obtain a discretized equation for the pressure field. Following the spirit of the Rhie and Chow interpolation procedure (Rhie and Chow, 1983), the pressure gradient ∇p and the gravity force are the only terms not assembled in $UEqn$. Hence, the goal of this method is to obtain a pressure equation ($pEqn$) by means of the mass conservation equation. Thus, either the incompressible or compressible mass equations (Equations 3 and 11) are discretized in the following form:

$$\sum_f (\mathbf{u})_f{}^n S_f = 0 \tag{24}$$

$$\sum_f (\rho\mathbf{u})_f{}^n S_f = -\frac{V_\mathrm{P}}{\Delta t}(\rho^n - \rho^{n-1}) \tag{25}$$

Taking advantage of the previously found velocity equations 21 and 22, the corresponding pressure equation are obtained:

$$\sum_{f=1}^{n} \left(\frac{1}{\rho_0}\frac{1}{a_\mathrm{P}}\right)_f \nabla \mathrm{P}_f \cdot S_f = \\ + \sum_{f=1}^{n} \left[\left(\frac{H(\mathbf{U})}{a_\mathrm{P}}\right)_f + \left(\frac{\rho\mathbf{g}}{\rho_0 a_\mathrm{P}}\right)_f\right] \cdot S_f \tag{26}$$

$$\sum_{f=1}^{n} \left(\frac{\rho}{a_\mathrm{P}}\right)_f \nabla p_{rgh_f} \cdot S_f = -\frac{V_\mathrm{P}}{\Delta t}\left(\rho^n - \rho^{n-1}\right) \\ + \sum_{f=1}^{n} \rho_f \left[\left(\frac{H(\mathbf{U})}{a_\mathrm{P}}\right)_f + \left(\frac{\mathbf{g}x\sum_f \rho^n}{a_{\mathrm{P}1}}\right)_f\right] \cdot S_f \tag{27}$$

2.5 Computational settings

Both 2D and 3D simulations were performed. The boundary conditions were no-slip for velocity and Neumann for pressure on the walls. Regarding thermal conditions, uniform and fixed temperatures were imposed to the heater (left) and cooler (right) walls. The remaining walls were assumed adiabatic. Despite closed domains were simulated, a reference pressure was set in an inner mesh cell. Pressure had no significant change for incompressible runs, whereas for compressible solutions it increased according with the increment of the average temperature of the fluid.

Pressure-based segregated transient solvers were used. A second order discretization scheme was chosen for the divergence terms and PIMPLE algorithm was selected for pressure-velocity coupling. The pressure was discretized with standard methods based on Rhie and Chow (Rhie and Chow, 1983); and second order scheme (Peng and Davidson, 2000) was employed to solve the $pEqn$.

Regarding the linear solver, the convergence criteria was achieved when the absolute residuals decreased below 10^{-6} or were three orders lower than the initial values. For PIMPLE convergence, the momentum predictor was not required. Two outer-PIMPLE iterations and four inner loop corrections were performed. Non-orthogonal correction was unnecessary because cartesian grids were employed.

Some variables such as the fluid average temperature T_{avr} and the wall heat flux at the hot (q_h) and cold (q_c) walls were selected for monitoring the convergence of the solutions. Once the monitor variables reached the steady state, the runs were continued for additional $1000s$ to obtain time-averaged field values. That allowed comparing the numerical transient simulations with the available experimental data.

3 RESULTS AND DISCUSSION

The first part of this section is concerned to simulate the Ampofo test (Ampofo and Karayiannis, 2003) by CFD. This problem consists of a air-filled *DHC* heated through the vertical walls with isolated horizontal walls. Figure 1 shows the test geometry. The domain is 0.75m height $\times$ 0.75m wide $\times$ 1.5m depth and the hottest wall is kept at $T_h = 50°C$ (left wall) whilst the coolest wall is kept at $T_c = 10°C$ (right wall). In the second part of this section, the Boussinesq approach is assessed for a very high Ra by solving the Ampofo test but using water as the working fluid in order to reach a very high Ra condition ($Ra = 4.1 \times 10^{11}$).

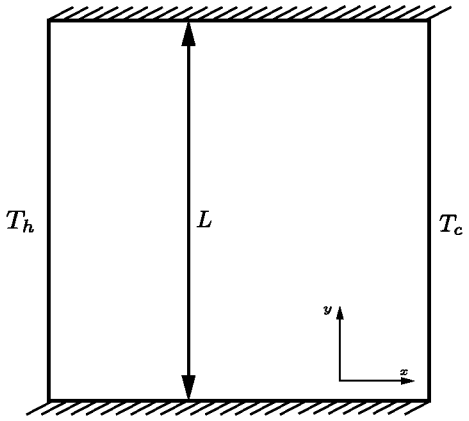

Figure 1: Sketch of the *DHC* test.

3.1 High Ra problem: air-filled cavity test

In this section the high Ra ($Ra = 1.59 \times 10^9$) Ampofo test (Ampofo and Karayiannis, 2003) was reproduced by 3D CFD. Calculations were performed for two meshes: the coarse mesh was $75 \times 75 \times 40$ (with mean $y+ = 3.42$ and a maximum value of 6.76 in the hot wall) and the finer mesh (named as $ref.$ in graphics) was $150 \times 150 \times 80$ (with mean $y+ = 1.53$ and a maximum value of 2.84 in the hot wall). Both grids were locally refined close to the walls. The maximum aspect ratio between the nearest wall cell and the core cells was 10. Despite the current mesh refinement, it is not enough to neglect turbulence modeling. However, the sub-grid viscosity (μ_{SGS}) is in the same order as the molecular viscosity, thus indicating that the influence of the unresolved scales on the solution is not critical. For this air-filled test $\mu = 1.6267 \times 10^{-5}$ and the average and maximum μ_{SGS} for the coarse mesh are 6.8190×10^{-7} and 4.35×10^{-5}, respectively. Regarding the finer mesh, the average and maximum values for μ_{SGS} become 1.8586×10^{-7} and 1.66×10^{-5}, respectively.

Figure 2a-b shows the dimensionless vertical velocity (V) and temperature (θ) over a horizontal mid-line crossing the cavity. Results correspond to the hot wall side for the velocity and the cold wall for the temperature. Good agreement is observed for the compressible solutions,

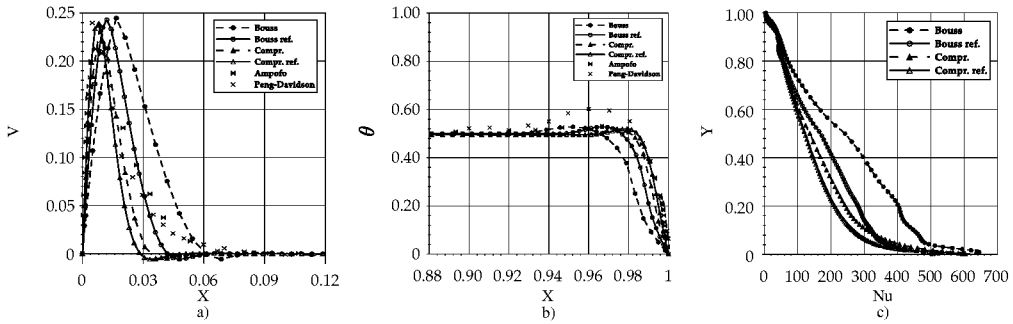

Figure 2: Mid-line ($Y = 0.5$, $Z = 0.5$) transport properties: a) Vertical dimensionless velocity ($V = vL/\alpha$), b) dimensionless temperature ($\theta = \frac{T-T_c}{T_h-T_c}$) and c) Nusselt distribution in the hot wall (Nu)

especially for the finest mesh (ref), although a less diffusive solution is found. In the cavity core ($0.1 < X < 0.9$) the velocity becomes almost negligible and temperature takes a constant value. Results follow the same trends as the ones obtained by Peng et al.(Peng and Davidson, 2000). The finer mesh solution ($Compr.ref.$) matches very well with the experimental data close to the wall but displays a velocity peak sharper than the Boussinesq solver. The Boussinesq approach results (named $Bouss$) show noticeable differences for the coarse mesh and the location of the velocity peak is incorrectly predicted. However, results get better for the the finest mesh. Discrepancies with the experimental data become significant a the right side of the velocity peak. Different from the results of Kizildag et al. (Kizildag et al., 2011), overestimation on the velocity peak was not evidenced for the compressible simulations.

The temperature distribution in figure 2-b shows good agreement for the finer meshes. The current results are better agreement than the reported by Peng et al.(Peng and Davidson, 2000). It should be noted that the core temperature is in all cases almost exactly the mean temperature T_{mw}. Comparing figures a and b, it can be noted that the flow layer and the thermal layer are of similar thickness ($\delta_f \approx \delta_t \approx 0.07$).

Figure 2-c shows the Nusselt number (Nu) in the hot wall for the compressible and Boussinesq solutions. For the finer mesh, the compressible solver gives slightly higher Nu at the bottom while a lower one in the rest of the wall. The heat flux transferred to the fluid presents a similar behavior than the observed in a previous study for lower Ra regimes (Corzo et al., 2011). By analyzing the behavior of the three displayed variables (V, θ and Nu) it is noticeable the influence of the grid resolution on the Boussinesq results. Moreover, agreement with compressible and experimental data clearly increases with mesh refinement. On the other hand, the compressible results seem to be less influenced by the mesh, although the finer mesh results are closer than experimental data. Nevertheless, it can be concluded that, for a sufficiently fine mesh, the Boussinesq approach is able to solve the current test.

Bibliography is rather contradictory about the air-cavity tests; LeQuere (Le Quéré, 1991) found that for a air-filled cavity the Boussinesq approach leads to asymmetrical flow results and Tian et al. (Tian and Karayiannis, 2000) reported that the air remains stationary between $Y = 0.25$ and 0.75 and reversal flow takes place towards the end of the boundary layers. On the contrary, Beghein et al. (Beghein et al., 1992) indicated that the air moves everywhere with the exception of the cavity core but no reversal flow is found. In the present results, antisymmetric patterns for V were found both for compressible and Boussinesq solutions. Reversal flow was

Table 1: Analyses cases

	T_c	T_h	ΔT	Ra	$\frac{\partial \rho}{\partial T}$	N_x	N_y	N_z	dim	$Turb.$
Test 1	10	50	40	4.1×10^{11}	Boussinesq	150	150	0	2D	laminar
Test 2	10	50	40	4.1×10^{11}	ρ real	150	150	0	2D	laminar
Test 3	10	90	80	8.2×10^{11}	ρ real	150	150	0	2D	laminar
Test 4	0	120	120	1.2×10^{12}	ρ real	150	150	0	2D	laminar
Test 5	10	50	40	4.1×10^{11}	Boussinesq	150	150	80	3D	LES
Test 6	10	50	40	4.1×10^{11}	ρ real	150	150	80	3D	LES
Test 7	10	50	40	4.1×10^{11}	ρ real	300	300	160	3D	LES

also identified in all numerical solutions although it is not shown for the experimental data from Ampofo.

3.2 Very high *Ra* problem: water-filled cavity test

In most industrial applications, where natural convection takes place, the flow is unsteady and turbulent with very high Ra and Re. Attending the lack of literature data for closed cavities at these regimes, some additional tests at very high Ra were performed. In these cases, the working fluid was water ($Pr = 5.42$) and simulations were carried out for three wall temperature ranges.

The cavity was solved with 2D and 3D domains and for the latter two different mesh refinements were implemented. Tests characteristics are summarized in Table 1 and itemized as:

- 2D domain: Tests 1 to 4 were performed on a square cavity of 0.75m height $\times$ 0.75m wide. Test 1 was solved with the Boussinesq approach while tests 2, 3 and 4 were solved with the compressible model. The accuracy of the Boussinesq approach was for a wide range of temperatures ($\Delta T = 40$, 80 and $120^{\circ}C$).

- 3D domain: Tests 5-7 were performed on a cavity of 0.75m height $\times$ 0.75m wide $\times$ 1.5m depth.

For the 2D cases the mesh was 150×150 quadratic cells (22.500 cells) with local refinement close to the walls. For these cases no turbulence model was considered. On the other hand, for the 3D cases two meshes were implemented; the coarse one with $150 \times 150 \times 80$ hexahedral cells (1.8×10^6 cells) and the finer one with $300 \times 300 \times 160$ hexahedral cells (14.4×10^6 cells) with the same refinement ratio near the walls. Similar than for the previous 3D cases, the subgrid scale viscosity μ_{SGS} was keep bounded. For example, for the test 1 the molecular viscosity μ was 7.968×10^{-4} while the average and maximum μ_{SGS} for the 3D coarse mesh (test 6) were 6.4302×10^{-5} and 1.34×10^{-2} respectively whereas for the finer mesh (test 7) they become 1.8373×10^{-5} and 4.98×10^{-3}, respectively.

Figure 3 shows the transient simulation for test 3. It can be concluded that the compressible model estimates a variation of density higher than that from the Boussinesq approach. Therefore, the buoyant force becomes higher near the walls affecting the flow behavior and enhancing the wall heat flux. Particularly, the heat flux in the hot wall (red line) is higher than in the cold-wall. However, this transient heat imbalance vanishes once the mean equilibrium

temperature (T_{avr}) is reached. This equilibrium temperature is higher than the mean wall temperature ($T_{avr} > T_{mw}$). As can be observed in figure 3-a, despite the equilibrium temperature is closer than the initial one, the evolution of T_{avr} is very slow and the simulated time has to be enough to reach steady-state conditions. In figure 3-b, the first two minutes of the transient simulation are shown. The mean temperature T_{avr} agrees with the global energy balance ($\int(\mathrm{P}_h - \mathrm{P}_c)dt = mCp\Delta T$). Thus, the mean temperature T_{avr} falls when the heat transfer in the cold wall is higher than in the hot wall, otherwise the mean temperature T_{avr} rises.

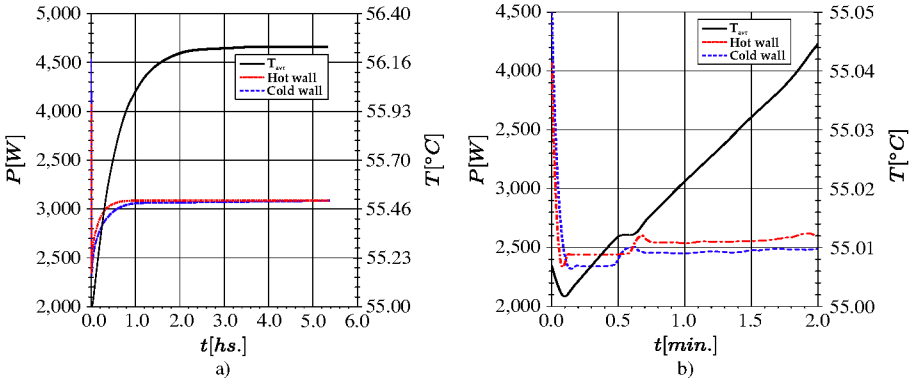

Figure 3: Transient results for test 3: a. Wall heat Power until to reach steady-state. b. Wall heat Power at the beginning of the simulation.

The dimensionless temperature $\theta = \frac{T-T_c}{T_h-T_c}$ is useful in order to compare the results obtained from the analyzed wall temperature ranges. The figure 4 shows the results obtained for the tests 1 to 4. The dimensionless temperature (θ) is displayed figure 4-a while the temperature difference $T_{\mathtt{diff}}$ ($T_{avr} - T_{mw}$) is shown in 4-b. Tests 1 and 2 allow comparing incompressible versus compressible solutions for $\Delta T = 40°C$ in the 2D domain. On the other hand, tests 2 to 4 are useful to evaluate how θ_{avr} grows from the Boussinesq solution $\theta_{mw} = 0.5$ while the ΔT increases. For Boussinesq approach (test 1) the mean temperature in the cavity core remains unchanged ($\theta_{avr} = \theta_{mw}$). On the contrary, for the compressible solver the T_{avr} grows until reaching a new equilibrium (e.g., for test 2 the final temperature θ grows up to 0.57). This trend is also found for tests 3 and 4, for which θ_{avr} = 0.60 and 0.62, respectively. Regarding the different temperatures obtained with the compressible and the Boussinesq approach, it is noticeable that the "error" introduced by the latter increases more than linearly with the temperature range.

Table 2 presents the difference temperature ($T_{\mathtt{diff}}$). As stated above, the differences grow faster than linearly with ΔT, i.e., for the lower ΔT ($40°C$) the compressible solver estimates a temperature $2.54°C$ upper than the expected; For the medium ΔT ($80°C$) it increases up to $6.24°C$ and finally for the larger ΔT ($120°C$) it is $11.81°C$. The relative error $\varepsilon_{\Delta T} = 100\frac{T_{\mathtt{diff}}}{\Delta T}$ with respect to the temperature range ΔT is calculated in the fifth column. In this case, the $\varepsilon_{\Delta T}$ increases linearly from around 6.35% for $\Delta T = 40°C$ up to 9.84% for $\Delta T = 120°C$.

As mentioned in the introduction section, a similar trend was found by Kizildag et al. (Kizildag et al., 2011) for a water-filled domain subjected to a temperature range of $10°C$. In this case $T_{\mathtt{diff}}$ was $0.75°C$, which is in agreement with the here reported value (see figure 4-b). It is remarkable that for compressible solution the average temperature becomes higher for 3D than 2D cases (compare test 2 vs tests 6 and 7). Considering that the 3D finer mesh case (test 7) should be the more accurate solution, then the error in Boussinesq approach solution grows up

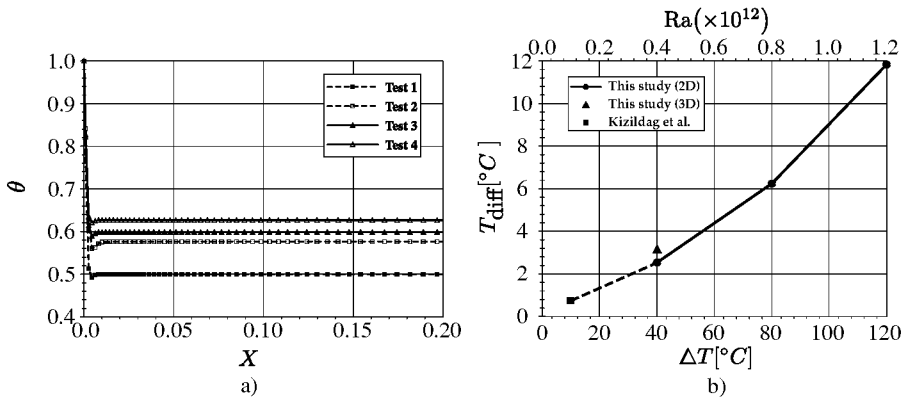

Figure 4: a. Mid-line ($Y = 0.5, Z = 0.5$) dimensionless temperature ($\theta = \frac{T-T_c}{T_h-T_c}$) for several temperature ranges. b. Difference between the average temperature ($T_{\texttt{diff}} = T_{avr} - T_{mw}$) from the compressible solver and the Boussinesq approach.

Table 2: Summarized results

Case	T_{avr}	T_{mw}	$T_{\texttt{diff}} = \lvert T_{avr} - T_{mw} \rvert$	$\varepsilon_{\Delta T}$
Test 1	303.00	303.00	0	0
Test 2	305.54	303.00	2.54	6.35
Test 3	329.24	323.00	6.24	7.80
Test 4	344.81	333.00	11.81	9.84
Test 5	303.00	303.00	0	0
Test 6	306.87	303.00	3.87	9.68
Test 7	306.11	303.00	3.11	7.77

to 7.77% for the lower temperature range analyzed. For sensible engineering applications such as nuclear industry, the Boussinesq approach shows a growing error in the mean temperature, exposing the limitations for solving liquid systems subject to typical temperature ranges.

In view of the results here reported and the results from Kizildag et al (Kizildag et al., 2011), it can be concluded that the error increases more than linearly with ΔT and consequently with the Rayleigh number. Therefore, it is possible to propose an empirical relationship for estimating the average-temperature error:

$$T_{\mathtt{diff}}(Ra) = 4.93\times10^{-24}Ra^2 + 4.072\times10^{-12}Ra - 0.2331 \quad \text{for} \quad 2.2\times10^{11} < Ra < 1.2\times10^{12} \tag{28}$$

$$T_{\mathtt{diff}}(\Delta T) = 0.000537\Delta T^2 + 0.03042\Delta T + 0.4132 \quad \text{for} \quad 10^{\circ}C < \Delta T < 120^{\circ}C \tag{29}$$

Equations 28 and 29 allow estimating the error in the average temperature using Boussinesq approach for a *DHC* and for water at very high *Ra* regime. Although the range of validity of these error estimation ($2.2\times10^{11} < Ra < 1.2\times10^{12}$ or $10^{\circ}C < \Delta T < 120^{\circ}C$) seems to be small, it is a novel validity criterion to be adopted for a water system subject to industrial conditions.

3D detailed simulations were carried on in order to arrive to a better understanding of the differences between both solvers and to study the 2D to 3D nature of the flow. To reduce the simulation time, the initial conditions were imposed from the previous 2D solutions.

Figure 5 shows the streamlines over two mid cut planes. Pictures 5-a and 5-b correspond to compressible and incompressible results respectively. In both cases a similar behavior is found and the flow presents a strong stratification along the vertical direction (see upper figures), which is characteristic of high *Ra* regime. On the other hand, significant differences seem to be found in the horizontal plane. However, these apparently large differences are easily explained by the fact that the horizontal transition plane, which is observed for both solvers, is placed in a slightly different height. The transition plane has negligible velocity and virtually divides the cavity in two parts. For Boussinesq simulations this plane exactly coincides with the horizontal mid plane at the middle of height ($Y = 0.5$), whereas, for the compressible model it is just a bit above.

Figure 6 shows the dimensionless horizontal velocity (U) and temperature (θ) over a vertical mid line. All tests results show significant in-core motion. For the Boussinesq results, the flow changes the direction exactly at the middle of height ($Y = 0.5$) while for compressible solutions the velocity inversion takes place at a slightly higher level. The Boussinesq approach gives perfectly antisymmetric solutions in the vertical direction both for U and θ. In this case, the near-wall velocity peak is 0.0055 at $Y = 0.0081$. On the other hand, compressible solutions are not completely antisymmetric. For instance, for test 7 the maximum velocities and the position where they occur (distance from wall) are different for bottom and top walls. The velocity peak near the top wall is $V = 0.004219$ at $Y = 0.01163$ while the peak near the bottom wall is slightly higher ($V = 0.005172$) and closer to the wall ($Y = 0.008637$).

Regarding the thermal distribution (see figure 6-b), both compressible solutions are similar. On the contrary, the Boussinesq approach displays a similar S-shape solution but with significant differences, especially in the core temperature.

Figure 7 shows the dimensionless vertical velocity (V) and temperature (θ) along a horizontal mid-line. The antisymmetric solutions for V and θ found for the Boussinesq approach are in accordance with the reported by Kizildag et al. (Kizildag et al., 2011). Regarding the velocity, perfectly antisymmetric solutions are found for both compressible and Boussinesq solvers. But,

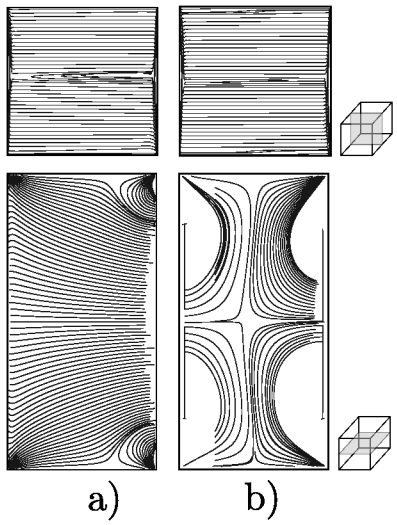

Figure 5: Streamlines in vertical (top) and horizontal (bottom) mean cut planes for: a. Compressible solver and b. Boussinesq approach.

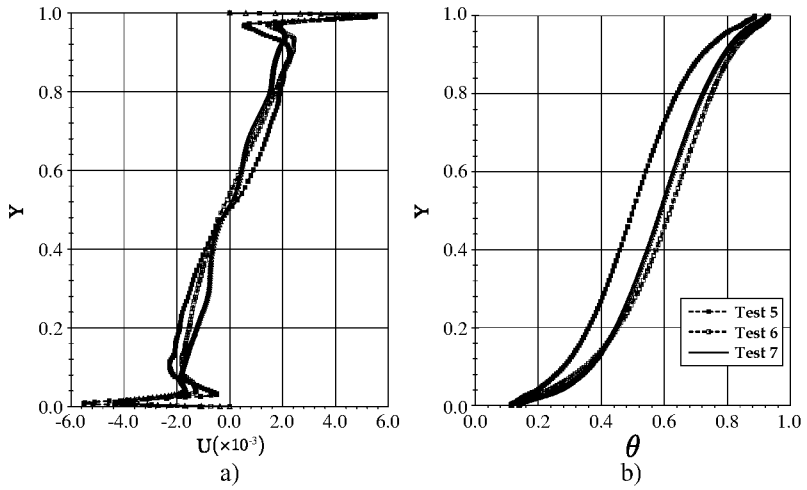

Figure 6: Mid-line ($X = 0.5$, $Z = 0.5$) transport properties for the Ampofo cavity using water as fluid: a) Dimensionless horizontal velocity ($U = uL/\alpha$) and b) Dimensionless temperature $\theta = \frac{T-T_c}{T_h-T_c}$

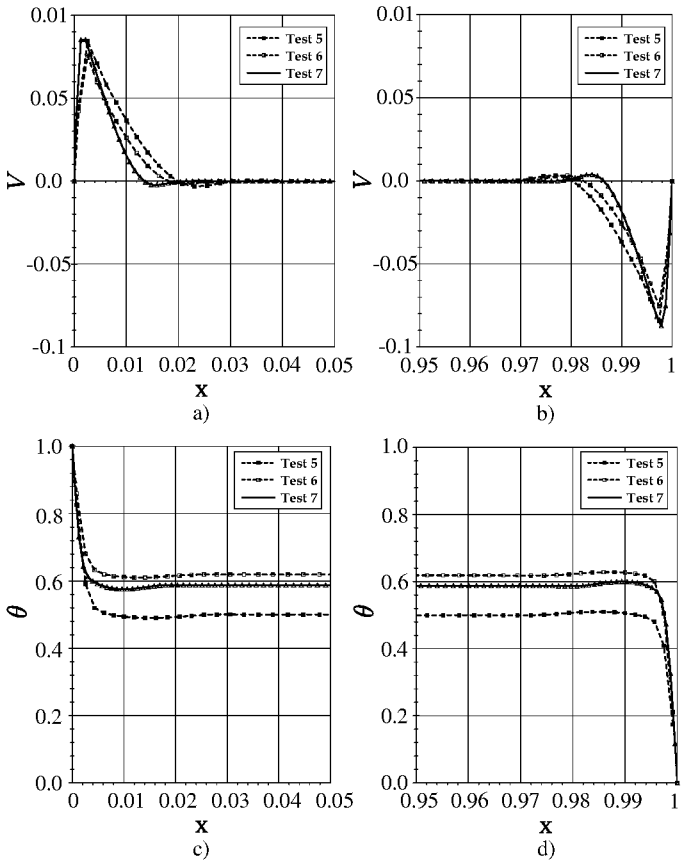

Figure 7: Transport variables along a mid-line ($Y = 0.5$, $Z = 0,5$): Dimensionless vertical velocity ($V = vL/\alpha$) close to the hot (a) and cold (b) walls, Dimensionless temperature $\theta = \frac{T-T_c}{T_h-T_c}$ close to the hot (c), and cold (d) walls

in really for the compressible solver the antisymmetric solution is obtained once the steady-state is reached and the equilibrium mean temperature is reached. On the contrary, for the Boussinesq solver the antisymmetric velocity pattern is found even during transient. Similar to air-filled cavity tests, for water the reversal flow is also evidenced close to the top and bottom walls and the flow layer thickness (δ_f) becomes thinner than for air. Moreover, δ_f is almost two times larger than the thermal layer thickness (δ_t) ($\delta_f \approx 0.03$ and $\delta_t \approx 0.018$). Because of that, the mesh requirements are harder to fulfill (Kizildag et al., 2011).

By comparing the vertical velocity profiles (V) in Figures 2 and 7 it is observed that the flow layer thickness (δ_f) is almost two times thinner for water than for air. This is consequence of two factors, first the higher viscosity of the water, which leads to a less diffusive solution, and second, the higher Ra of the water test. In a previous work (Corzo et al., 2011), the authors demonstrated that the flow layer thickness is inversely proportional to the Ra. Similarly, δ_t is four times thinner for water than for air.

The local Nusselt number (Nu) is shown in figure 8. Both solvers arrived to similar results. The Nu distribution for water presents the same trend than for air although the average Nu ($\langle Nu \rangle$) is significant larger ($\langle Nu \rangle_{water} = 805.4$ and $\langle Nu \rangle_{air} = 138.4$).

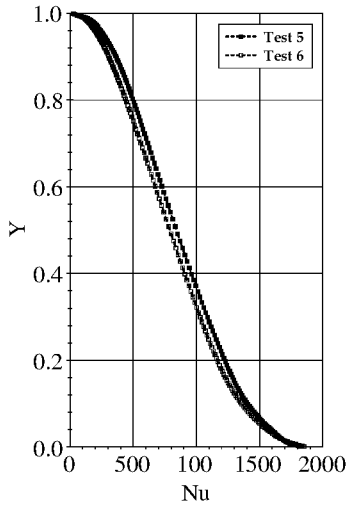

Figure 8: Nusselt distribution in the hot wall (Nu)

3.3 Thermal stratification for different Rayleigh number

Thermal stratification can be quantified by calculating the average temperature gradient along the vertical direction. This is called stratification parameter (S) and is frequently reported in experimental and numerical studies. A detailed overview of numerical test data can be found in Salat et al. (Salat et al., 2004). Recently Trias et al. (Trias et al., 2010) and Saury et al. (Saury et al., 2011) carried out experimental studies with optical access devices and found that the thermal radiation and the emissivity of the glass windows has a significant incidence on the stratification and could lead to discrepancies in the measuring data. Saury et al.(Saury et al., 2011) studied the influence of the wall emissivity in air-filled problems at high Ra ($Ra > 10^{10}$), concluding that S is slightly modified by changing the Ra from 5.8×10^{10} to 1.02×10^{11}. However, this conclusion is only valid for a narrow range of high Ra. The numerical results obtained

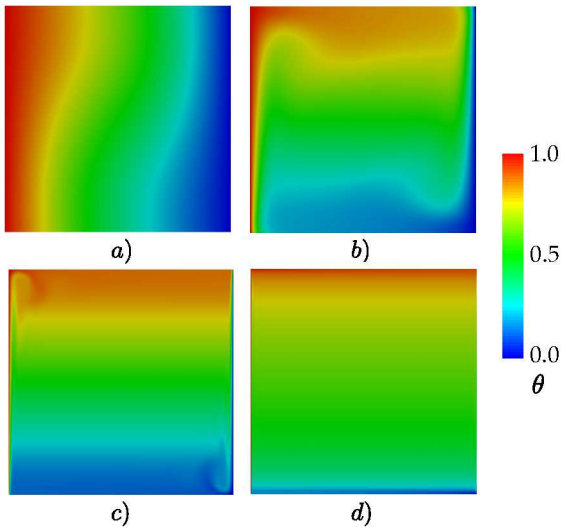

Figure 9: Dimensionless temperature field $\theta = \frac{T-T_c}{T_h-T_c}$. a) $Ra = 10^3$, b) $Ra = 10^6$, c) $Ra = 1.59 \times 10^9$ and d) $Ra = 4.1 \times 10^{11}$

in the present work, covering a wide range of Ra from 10^3 to 4×10^{11}, display a very strong relationship between S and Ra. Figure 9 shows the temperature distribution obtained using the Boussinesq approach in three air-filled cavity tests at $Ra = 10^3$ (low Ra), $Ra = 10^6$ (medium Ra), $Ra = 1.59 \times 10^9$ (high Ra) and one water-filled cavity test at $Ra = 4 \times 10^{11}$ (very high Ra). The two lower results correspond to previously reported data ((Corzo et al., 2011)), but are useful to visualize the stratification evolution as Ra increases. Accordingly, it can be concluded that stratification increases with Rayleigh, and problems dominated by natural convection at very high Ra are characterized by a high thermal stratification in the vertical direction. Figure 10 illustrates the above mentioned.

Figure 10-a shows the averaged stratification $\langle S_{1D} \rangle$ (along the vertical mid line) as a Ra function. Thermal conduction dominates the heat transfer phenomena for low Ra, but between $10^3 < Ra < 10^4$ the problem becomes purely convective. Thus, stratification reaches values above $\langle S \rangle > 0.6$ for $Ra > 10^4$.

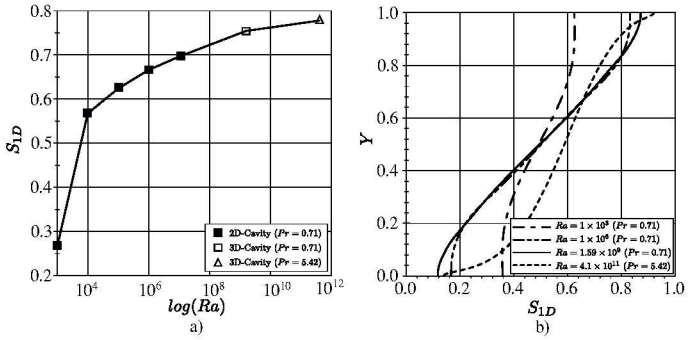

Figure 10: Stratification description: a) Stratification parameter S_{1D} as a function of the Rayleigh number, b) Dimensionless temperature θ along the vertical coordinate

Table 3: Stratification parameter

Case	$\langle S \rangle$	S_{1D}
Test 1	1.1174	0.8310
Test 2	1.1932	0.8882
Test 3	1.1817	0.8802
Test 4	1.1524	0.8572
Test 5	1.0474	0.7731
Test 6	1.1001	0.8141
Test 7	1.0586	0.7799

Figure 10-b shows the S_{1D} distribution along the vertical mid line. It should be noted that the air-filled cavity cases (Ra = 10^3, 10^6 and 1.59×10^9) have the same S-shape solution while the water-filled cavity shows the opposite shape.

For this height aspect ratio ($A_h = 1$) the stratification seems to be asymptotic to 1 while Ra grows (see figure 10-a). In this sense, Saury et al.(Saury et al., 2011) found that the height aspect ratio and the wall emissivity play the most important role: Stratification (S) decreases as long as wall radiation increases. In concordance with Saury et al., Salat et al.(Salat et al., 2004) found that for a cubic cavity (aspect ratio A_h = 1) and $Ra = 1.48 \times 10^9$ the stratification parameter changes from $S = 0.52$ to 0.72 by changing the emissivities of the optical windows from $\varepsilon = 0.95$ to 0.1 respectively. The current simulations were performed without taking into account the radiation heat transfer ($\varepsilon = 0.0$). Under this condition, the stratification parameter was quite similar for both solvers ($S = 0.779$ for compressible and $S = 0.773$ for Boussinesq), which is in very good agreement with the obtained by Salat(Salat et al., 2004) for low emissivity tests.

It can be noted that the spatial-average stratification $\langle S \rangle$ is substantially different to that computed in the vertical mid line S_{1D}. Table 3 summarized both parameters for all the very high Ra cases.

3.4 Fluid density approaches

Returning to the incompressible momentum equation (Eqn. 7) and looking at the definition of β in Eqn. 8, the different buoyancy forces in the heating walls depends mainly on the change of $\partial\rho/\partial T$. That is, for fluids having low dependence of density with temperature, or for systems operating within narrow temperature ranges, β will be nearly constant. On the other hand, for typical liquids operating within large temperature ranges the variation of β will be significant.

The figure 11-a shows the derivative of the water density with respect to the temperature ($\partial\rho/\partial T$) and the corresponding thermal expansion coefficient β. The figure 11-b at the upper side shows the variation of the density for the range of studied temperatures along with the three tangent lines at the T_{mw} of each temperature range. The problems are evidenced when the curvature of the density ($\partial^2\rho/\partial T^2$) becomes significant. In these cases the first order linear estimation assumed by the Boussinesq approach is no longer enough to calculate the density changes accurately, and the approach error quickly increases with the temperature range. Lets exemplify that for two typical fluids, air and water, subjected to the currently studied temperature ranges ($\Delta T = 40°C$, $80°C$ and $120°C$). Figure 12 shows the relative error on the density estimation (ρ_{est}) for the cold and hot wall temperatures (T_c and T_h), obtained by using first

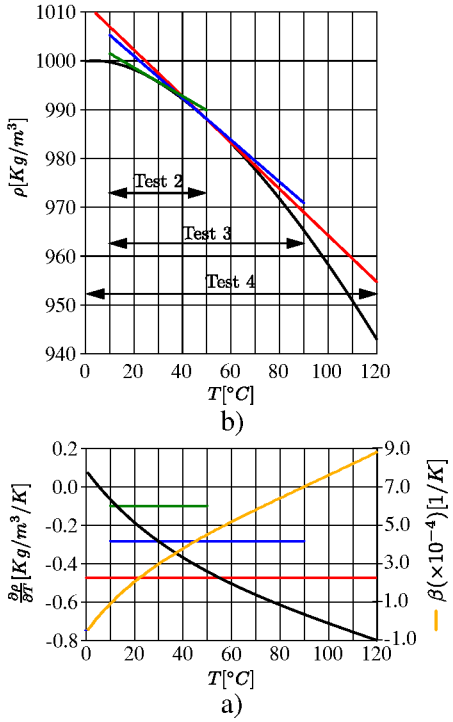

Figure 11: Thermal properties: a. Derivative of density (left vertical axis) and thermal expansion coefficient (right vertical axis) distribution with respect to the temperature, b. Variation of density along the analyzed temperature ranges.

(Boussinesq), second and third order Taylor series approaches. The relative errors were calculated based on the exact density variation between the mean and the wall temperatures ($\varepsilon_r = \left| \frac{\rho_{est} - \rho}{(\rho - \rho_{mw})_{exact}} \right|$). As can be noted, for water cases the linear approach introduces errors higher than 20% for all the temperature ranges ΔT. On the other hand, a noticeable improvement is obtained by increasing the approach order. For air cases, the linear approach leads to acceptable estimations for the lower temperature range ($\Delta T = 40°$), although the errors meaningful increases for the other cases. However, ε_r quickly decreases for second order approach getting suitable estimations.

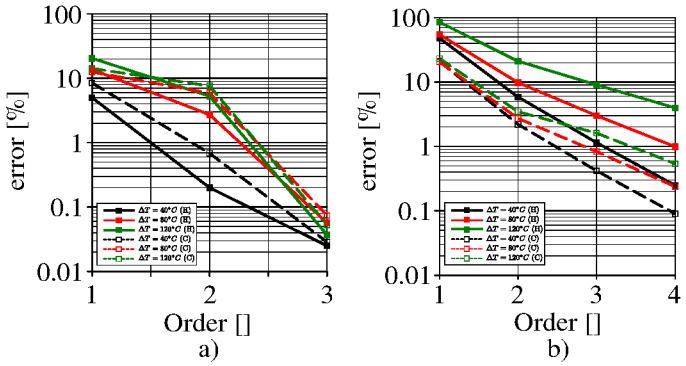

Figure 12: Level of approaches for density calculation: a. Air fluid, b. Water fluid.

This analysis is an easy and fast way to have a first estimation about the suitability of the Boussinesq approach for solving a given problem. Nevertheless, future work would be devoted to understand how these estimation errors impact over the fluidynamic results. The implementation of a high-order Boussinesq approach should also be investigated.

4 CONCLUSIONS

In the present work, a rigorous numerical study concerning to natural convection heat transfer and the Boussinesq approach validity was carried out. The assessment was focused on high and very high Rayleigh numbers (*Ra*) in Differentially Heated Cavities (*DHC*). This widely studied cavity problem was solved with the incompressible Boussinesq approach and a compressible solver. The comparison with experimental data was only possible for the air-filled case ($Ra = 1.59 \times 10^9$), finding good agreement. For water-filled cases ($4.1 \times 10^{11} < \mathrm{Ra} < 1.2 \times 10^{12}$) some differences between both solvers were found. On the one hand, the incompressible solver gave the expected perfectly antisymmetrical results. The heat fluxes at the cold and hot walls were exactly the same throughout the simulation time. Consequently, the steady-state average temperature was the mean temperature between the walls. On the other hand, the compressible solver reproduced the real non-linear relationship between temperature and density. As a result, a transient heat flux imbalance between cold and hot walls took place initially and continued until the system reached steady-state conditions, reaching an average temperature higher than that found with the Boussinesq approach. This behavior is less evidenced for air-filled *DHC* (even for high *Ra*), but noticeable for water-filled *DHC* at very high *Ra*. That allows concluding that a validity criterion for the Boussinesq approach should attend to the admissible errors of heat transfer and velocity but also to the average temperature error. In this work, a novel validity criterion for water system subject to very high *Ra* and/or operating temperature ranges was

proposed based on the obtained numerical results.

Regarding the thermal pattern, stratification increased as long as the *Ra* increases, changing from horizontal stratification for low *Ra* to vertical stratification for very high *Ra*. That is, for low and medium *Ra* the temperature gradient is directed from the cold wall to the hot one. On the contrary, for high and very high *Ra*, the gradient is oriented from the bottom to the top of the domain.

According to numerical evidence found in the current work, it can be concluded that the Boussinesq approach is suitable only if the fluid density variation around the average temperature is small enough to justify its inherent linear assumption. For air systems, the Boussinesq approach seems to be suitable even for high *Ra* problems. On the contrary, for water systems working at typical temperature ranges (several tens of degrees or hundreds of degrees) the fluid average temperature could be farther than the expected. In particular, especial care should be taken for systems such as nuclear reactors vessels, which work within a wide operation temperature range. In these systems the average temperature have to be accurately defined to design the control and safety systems. Therefore, the Boussinesq approach could lead to fluid temperature underestimation if fixed temperature boundary conditions are applied. Additional work should be done in order to improve the original Boussinesq Approach by using a more accurate second order approach for density.

ACKNOWLEDGEMENTS

The authors would like to thank the CONICET (PIP 112 201101 00331) and ANPCyT (PICT 2013-830) and Universidad Nacional del Litoral (CAI+D 2011 PJ 500 201101 00015 and CAI+D PI 501 201101 00435) for giving the financial support for carring on this research. Lastly, thanks should be given to Nicolas Schiliuk, who contributed significantly to improve this study.

REFERENCES

Ampofo F. and Karayiannis T. Experimental benchmark data for turbulent natural convection in an air filled square cavity. *International Journal of Heat and Mass Transfer*, 46(19):3551–3572, 2003.

Aydin O. and Yang W. Natural convection in enclosures with localized heating from below and symmetrical cooling from sides. *International Journal of Numerical Methods for Heat & Fluid Flow*, 10(5):518–529, 2000.

Barhaghi D. and Davidson L. On the validity of the boussinesq approximation in a developing mixed convection boundary layer. In *2007 International Conference on Thermal Issues in Emerging Technologies: Theory and Application*, pages 183–190. IEEE, 2007.

Barhaghi D., Davidson L., and Karlsson R. Large-eddy simulation of natural convection boundary layer on a vertical cylinder. *International journal of heat and fluid flow*, 27(5):811–820, 2006.

Basit M., Rafique M., Chughtai I., and Inayat M. Computer simulation of natural convection heat transfer from an assembly of vertical cylinders of parr-2. *Applied thermal engineering*, 27(1):194–201, 2007.

Becker R. and Braack M. Solution of a stationary benchmark problem for natural convection with large temperature difference. *International journal of thermal sciences*, 41(5):428–439, 2002.

Beghein C., Allard F., and Draoui A. Numerical modelling of turbulent convection in a

thermally-driven square cavity. In *Turbulent Natural Convection in Enclosures-A Computational and Experimental Benchmark Study, Proceedings of the Eurotherm Seminar Delft, The Netherlands*, 22, pages 31–42. 1992.

Corzo S., Damián S., Ramajo D., and Nigro N. Numerical simulation of natural convection phenomena. *Mecánica Computacional*, 30:277–296, 2011.

Darbandi M. and Hosseinizadeh S.F. Numerical simulation of thermobuoyant flow with large temperature variation. *Journal of thermophysics and heat transfer*, 20(2):285–296, 2006.

De Vahl Davis G. Natural convection of air in a square cavity: a bench mark numerical solution. *International Journal for Numerical Methods in Fluids*, 3(3):249–264, 1983.

Ferziger J.H. and Peric M. *Computational methods for fluid mechanics*, volume 5. 2002.

Gray D.D. and Giorgini A. The validity of the boussinesq approximation for liquids and gases. *International Journal of Heat and Mass Transfer*, 19(5):545–551, 1976.

Henkes R. and Le Quéré P. Three-dimensional transition of natural-convection flows. *Journal of Fluid Mechanics*, 319:281–303, 1996.

Hung K.S. and Cheng C.H. Pressure effects on natural convection for non-boussinesq fluid in a rectangular enclosure. *Numerical Heat Transfer: Part A: Applications*, 41(5):515–528, 2002.

Jiang Y.Y., Shoji M., and Naruse M. Boundary condition effects on the flow stability in a toroidal thermosyphon. *International Journal of Heat and fluid flow*, 23(1):81–91, 2002.

Kizildag D., Rodríguez Pérez I.M., and Oliva Llena A. On the validity of the boussinesq approximation in a tall differentially heated cavity with water. In *7th International Conference on Computational Heat and Mass Transfer*, pages 1–7. 2011.

Krishnani M. and Basu D.N. On the validity of boussinesq approximation in transient simulation of single-phase natural circulation loops. *International Journal of Thermal Sciences*, 105:224–232, 2016.

Kumar P. and Eswaran V. A numerical simulation of combined radiation and natural convection in a differential heated cubic cavity. *Journal of Heat Transfer*, 132(2):023501, 2010.

Le Quéré P. Accurate solutions to the square thermally driven cavity at high rayleigh number. *Computers & Fluids*, 20(1):29–41, 1991.

Le Quéré P. and Behnia M. From onset of unsteadiness to chaos in a differentially heated square cavity. *Journal of Fluid Mechanics*, 359:81–107, 1998.

Mlaouah H., Tsuji T., and Nagano Y. A study of non-boussinesq effect on transition of thermally induced flow in a square cavity. *International Journal of Heat and Fluid Flow*, 18(1):100–106, 1997.

Navamani R. and Murugan N. Numerical study of buoyancy-driven transitional flow in a square cavity with partially heated and cooled vertical walls. *International Journal of Numerical Methods for Heat & Fluid Flow*, 20(7):744–758, 2010.

Patterson J. and Imberger J. Unsteady natural convection in a rectangular cavity. *J. Fluid Mech*, 100(1):65–86, 1980.

Peng S. and Davidson L. Numerical investigation of turbulent buoyant cavity flow using large eddy simulation. In *Int. Symp. Turbulence Heat Mass Transfer*, volume 3, pages 737–744. 2000.

Pesso T. and Piva S. Laminar natural convection in a square cavity: low prandtl numbers and large density differences. *International Journal of Heat and Mass Transfer*, 52(3):1036–1043, 2009.

Rasoul J. and Prinos P. Natural convection in an inclined enclosure. *International Journal of Numerical Methods for Heat & Fluid Flow*, 7(5):438–478, 1997.

Rhie C. and Chow W. Numerical study of the turbulent flow past an airfoil with trailing edge

separation. *AIAA*, 21:1525–1532, 1983.

Salat J., Xin S., Joubert P., Sergent A., Penot F., and Le Quere P. Experimental and numerical investigation of turbulent natural convection in a large air-filled cavity. *International journal of heat and fluid flow*, 25(5):824–832, 2004.

Saury D., Rouger N., Djanna F., and Penot F. Natural convection in an air-filled cavity: Experimental results at large rayleigh numbers. *International Communications in Heat and Mass Transfer*, 38(6):679–687, 2011.

Smagorinsky J. General circulation experiments with the primitive equations. 1.the basic experiment. *Mon. Weather Rev.*, 91:99–164, 1963.

Tian Y. and Karayiannis T. Low turbulence natural convection in an air filled square cavity:: Part i: the thermal and fluid flow fields. *International Journal of Heat and Mass transfer*, 43(6):849–866, 2000.

Trias F., Gorobets A., Soria M., and Oliva A. Direct numerical simulation of a differentially heated cavity of aspect ratio 4 with rayleigh numbers up to 10 11–part i: Numerical methods and time-averaged flow. *International Journal of Heat and Mass Transfer*, 53(4):665–673, 2010.

Trias F., Soria M., Oliva A., and Pérez-Segarra C. Direct numerical simulations of two-and three-dimensional turbulent natural convection flows in a differentially heated cavity of aspect ratio 4. *Journal of Fluid Mechanics*, 586:259–293, 2007.

Tsuji T. and Nagano Y. Turbulence measurements in a natural convection boundary layer along a vertical flat plate. *International journal of heat and mass transfer*, 31(10):2101–2111, 1988.

Van Driest E.R. On turbulent flow near a wall. *Journal of the Aeronautical Sciences (Institute of the Aeronautical Sciences)*, 23(11), 2012.

Versteeg H.K. and Malalasekera W. *An introduction to computational fluid dynamics: the finite volume method*. Pearson Education, 2007.

Vierendeels J., Merci B., and Dick E. A multigrid method for natural convective heat transfer with large temperature differences. *Journal of computational and applied mathematics*, 168(1):509–517, 2004.

Wagner W. and Pruß A. The iapws formulation 1995 for the thermodynamic properties of ordinary water substance for general and scientific use. *Journal of Physical and Chemical Reference Data*, 31(2):387–535, 2002.

Zhong Z., Yang K., and Lloyd J. Variable property effects in laminar natural convection in a square enclosure. *Journal of Heat Transfer*, 107(1):133–138, 1985.

Zvirin Y. A review of natural circulation loops in pressurized water reactors and other systems. *Nuclear Engineering and Design*, 67(2):203–225, 1982.

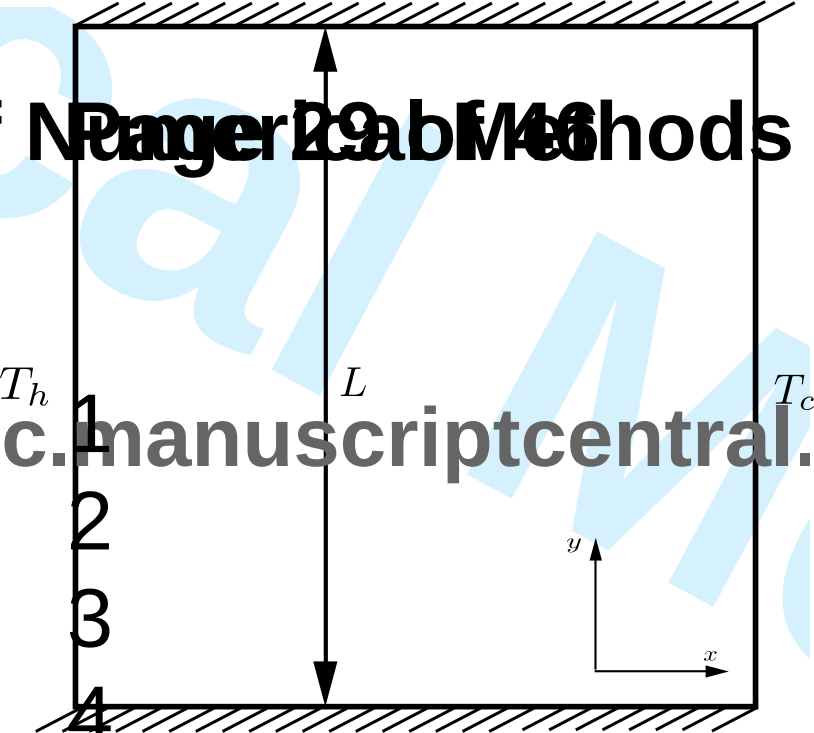

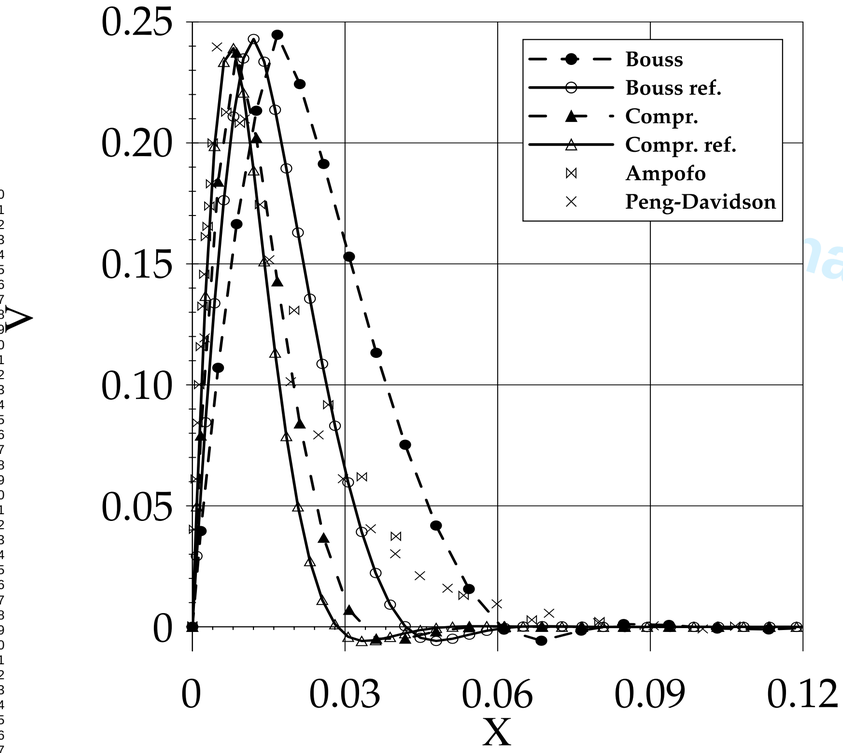

a)

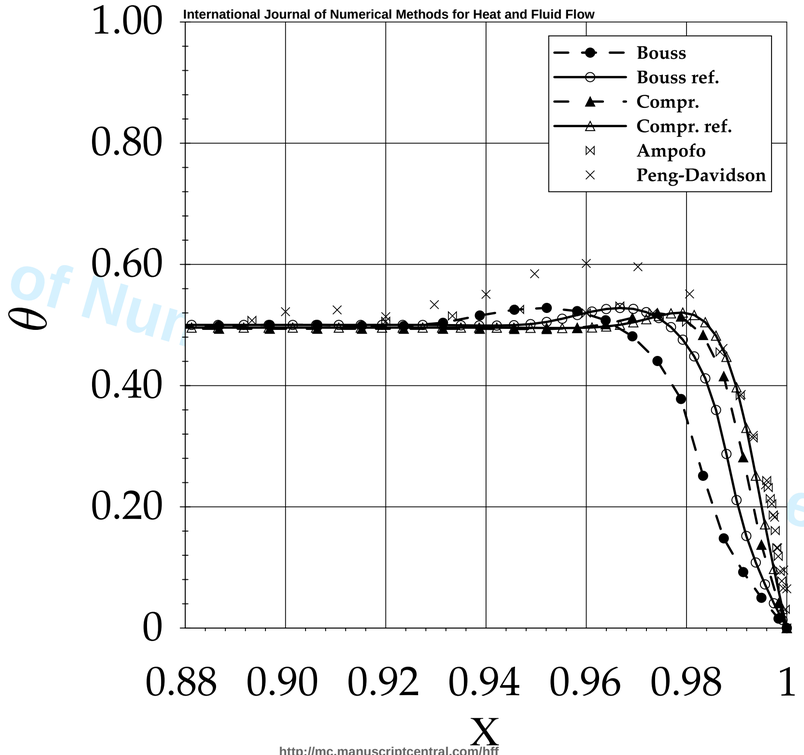

b)

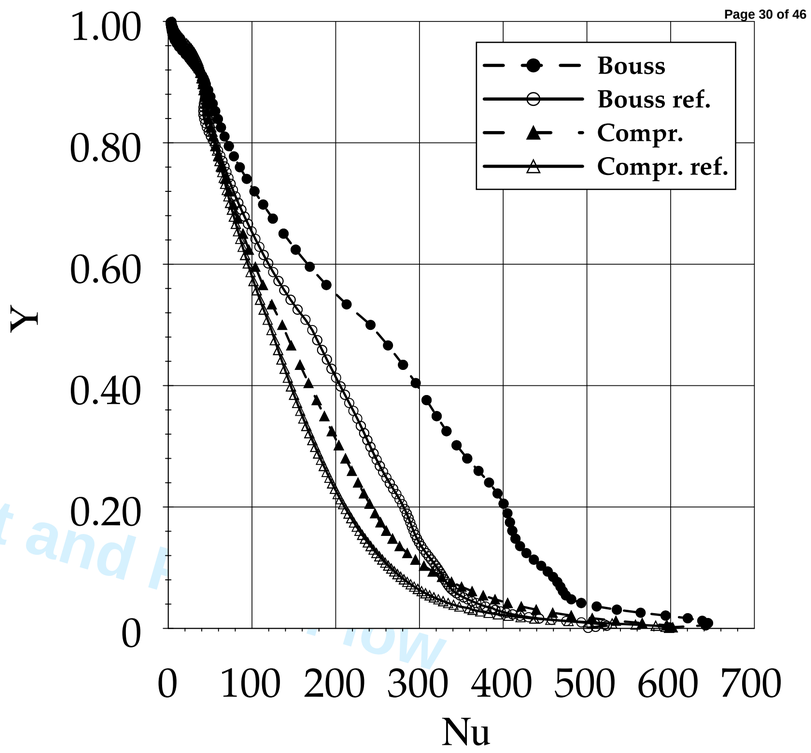

c)

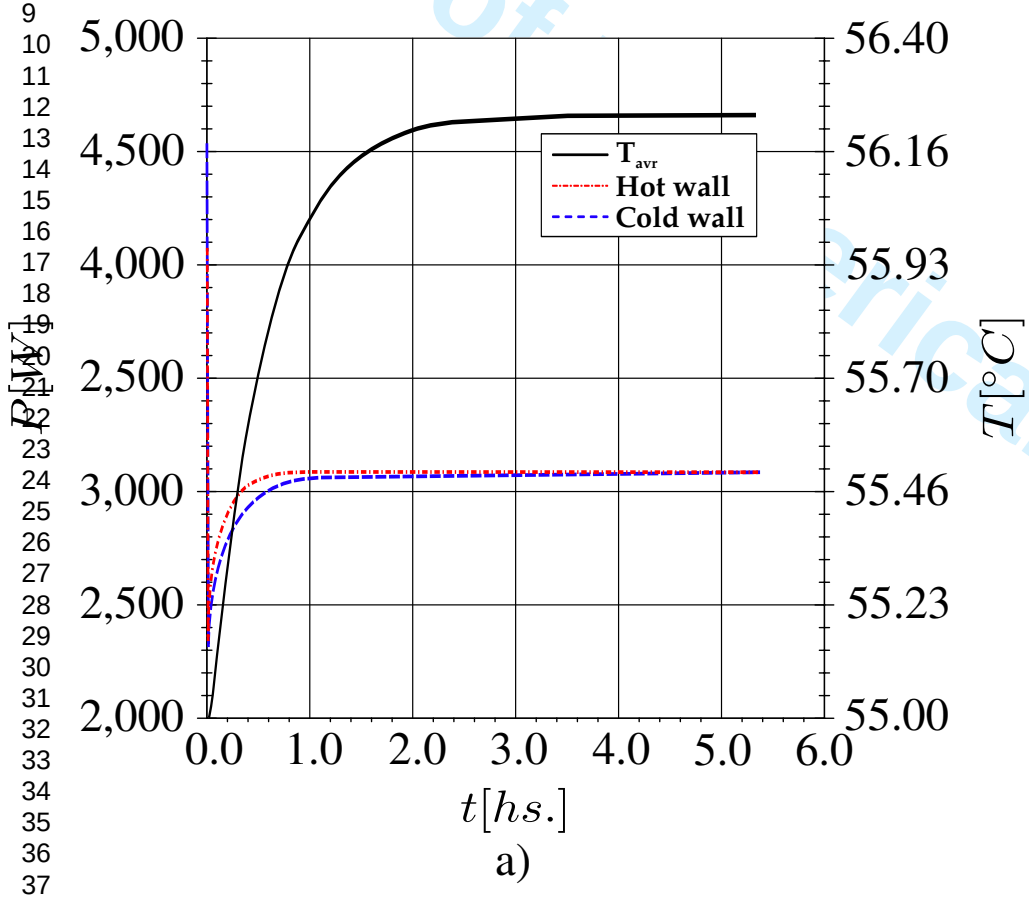
5,000
4,500
4,000
2,500
3,000
2,000
56.40
56.16
55.93
55.70
55.46
55.23
55.00
0.0
1.0
2.0
3.0
4.0
5.0
6.0
$t[hs.]$
$P[W]$
$T[°C]$
T_{avr}
Hot wall
Cold wall

a)

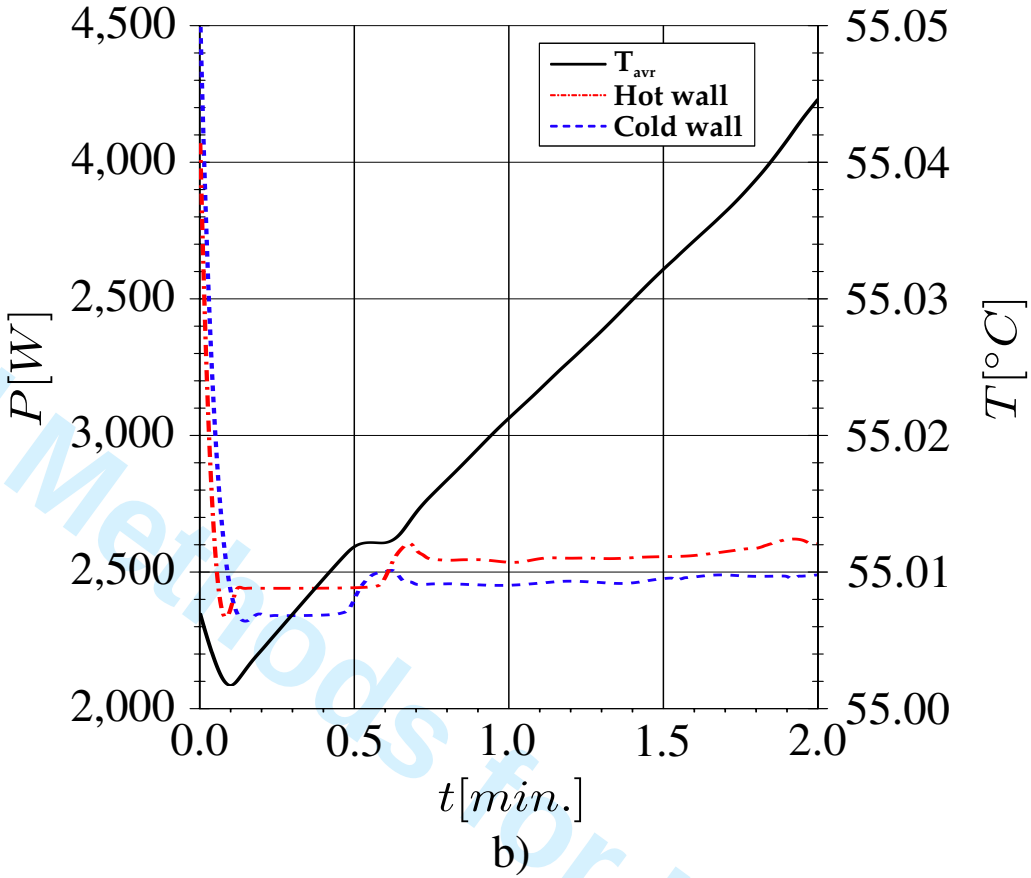
4,500
4,000
2,500
3,000
2,500
2,000
55.05
55.04
55.03
55.02
55.01
55.00
0.0
0.5
1.0
1.5
2.0
$t[min.]$
$P[W]$
$T[°C]$
T_{avr}
Hot wall
Cold wall

b)

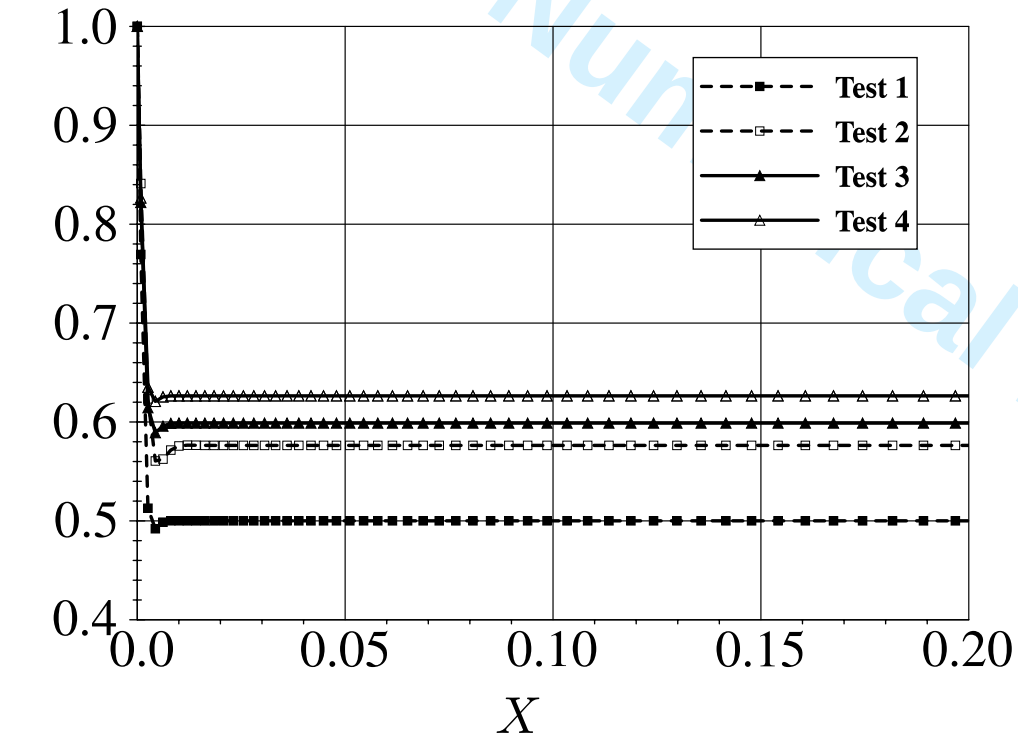
Test 1
Test 2
Test 3
Test 4
1.0
0.9
0.8
0.7
0.6
0.5
0.4
0.0
0.05
0.10
0.15
0.20
Y
X

a)

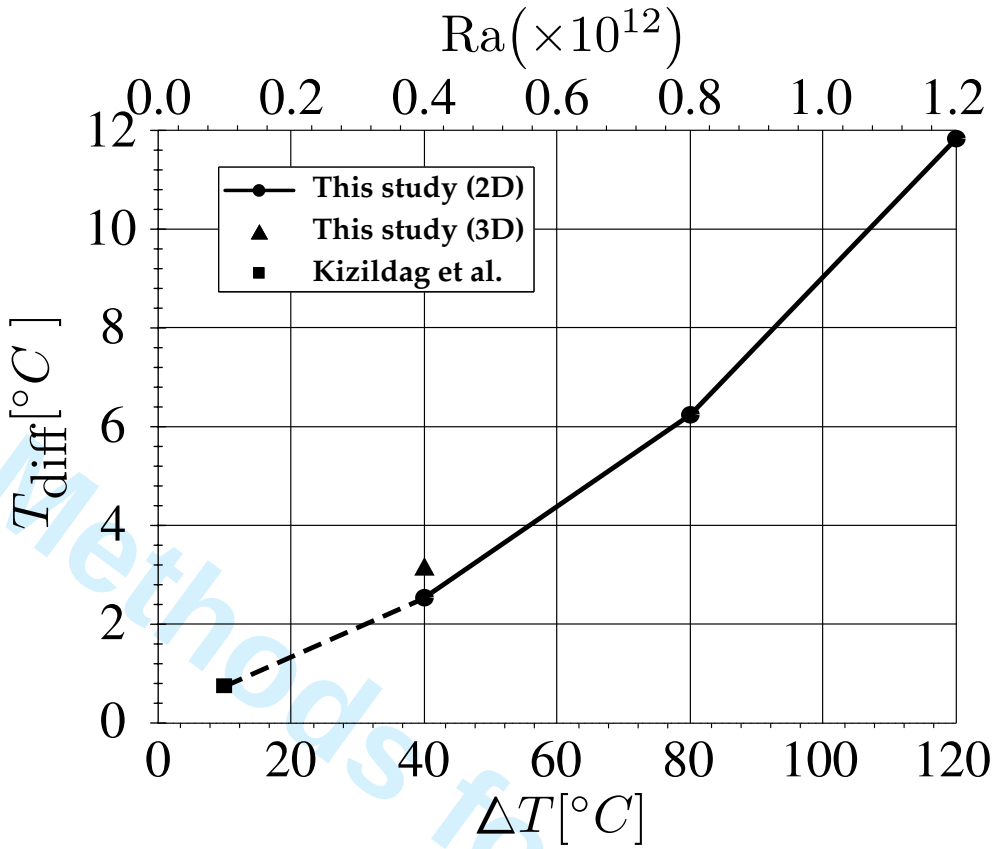
Ra(×10^12)
0.0
0.2
0.4
0.6
0.8
1.0
1.2
This study (2D)
This study (3D)
Kizildag et al.
12
10
8
6
4
2
0
0
20
40
60
80
100
120
T_diff[°C]
ΔT[°C]

b)

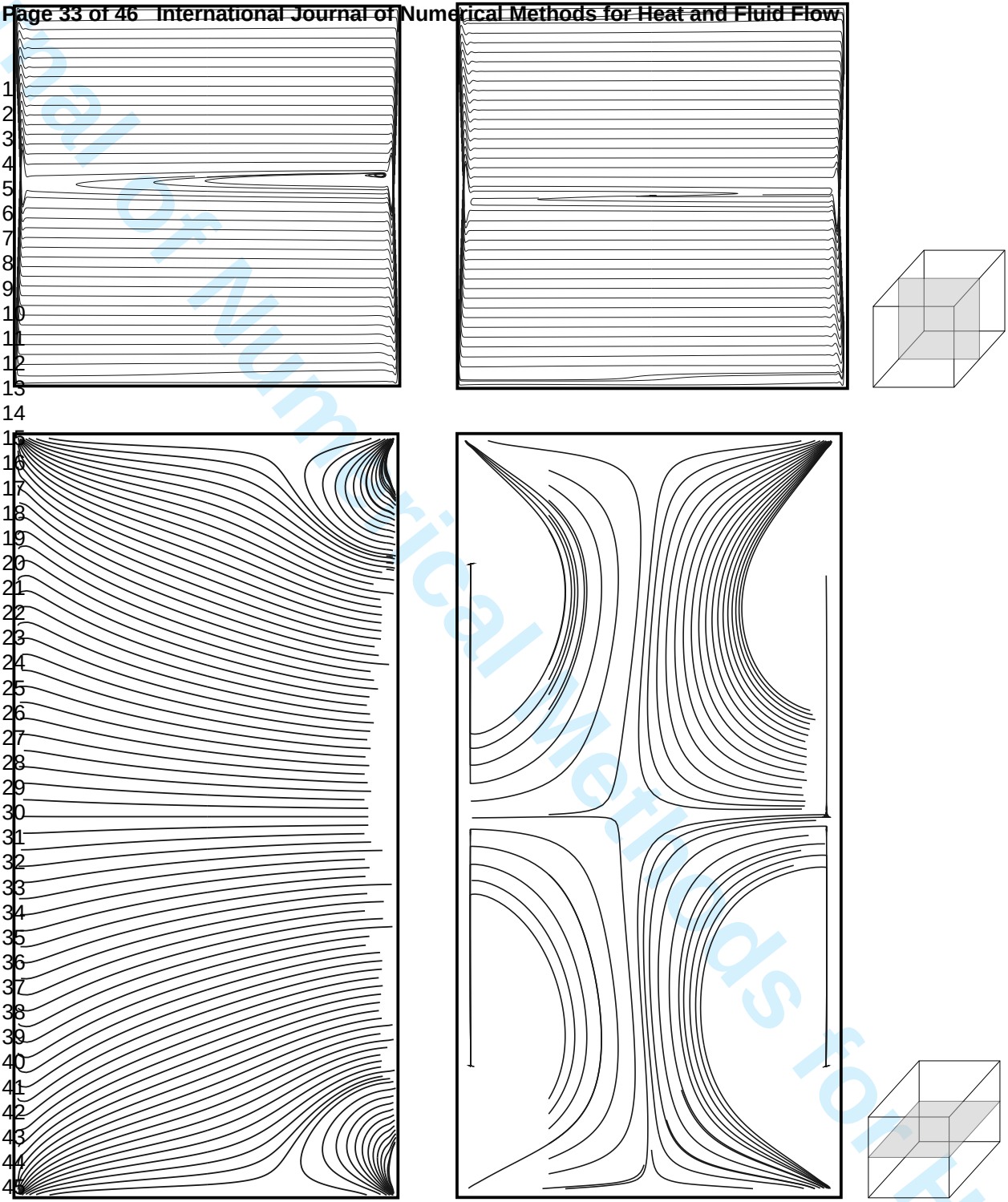

a) b)

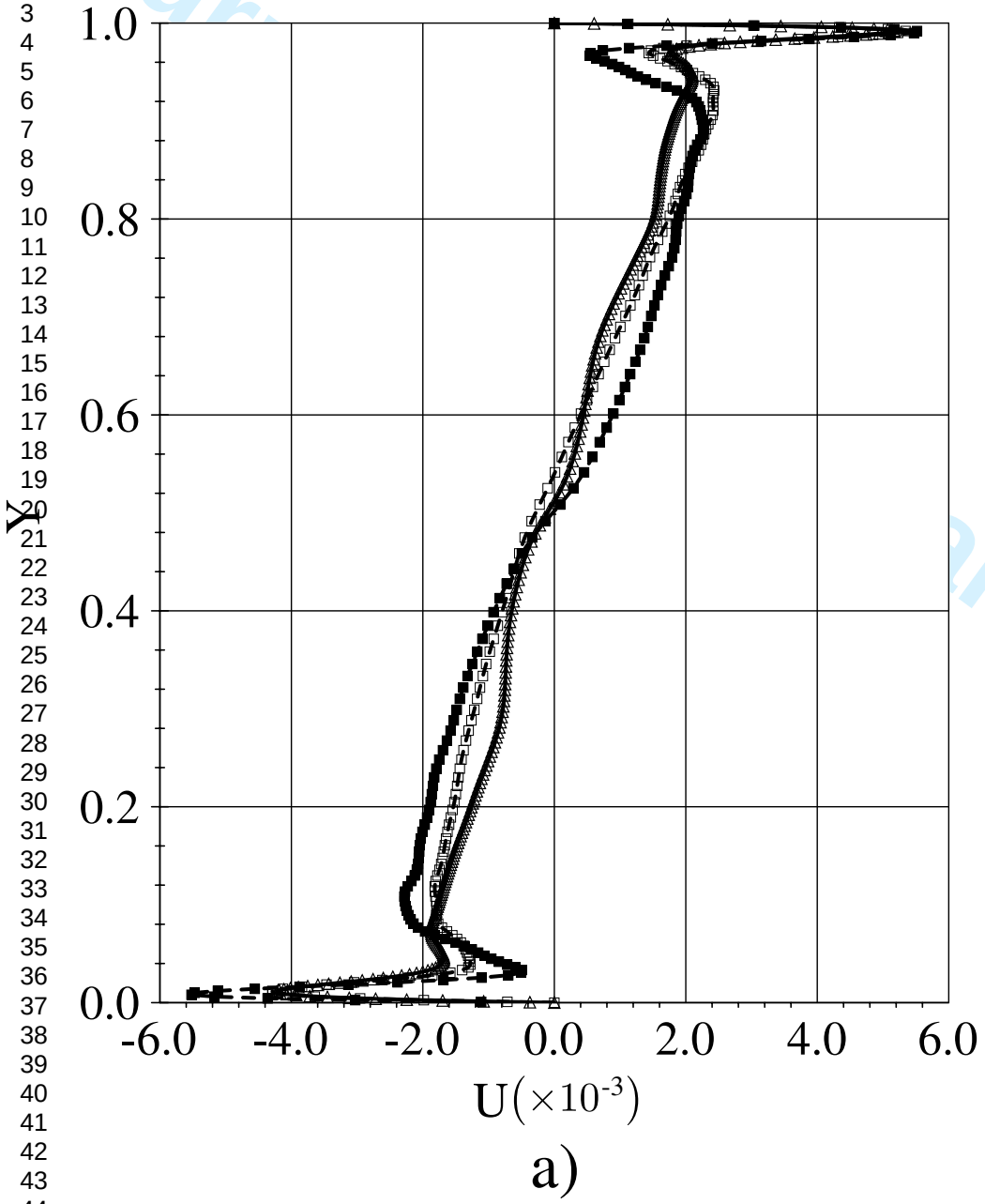
1.0
0.8
0.6
0.4
0.2
0.0
Y
-6.0
-4.0
-2.0
0.0
2.0
4.0
6.0
U(×10-3)

a)

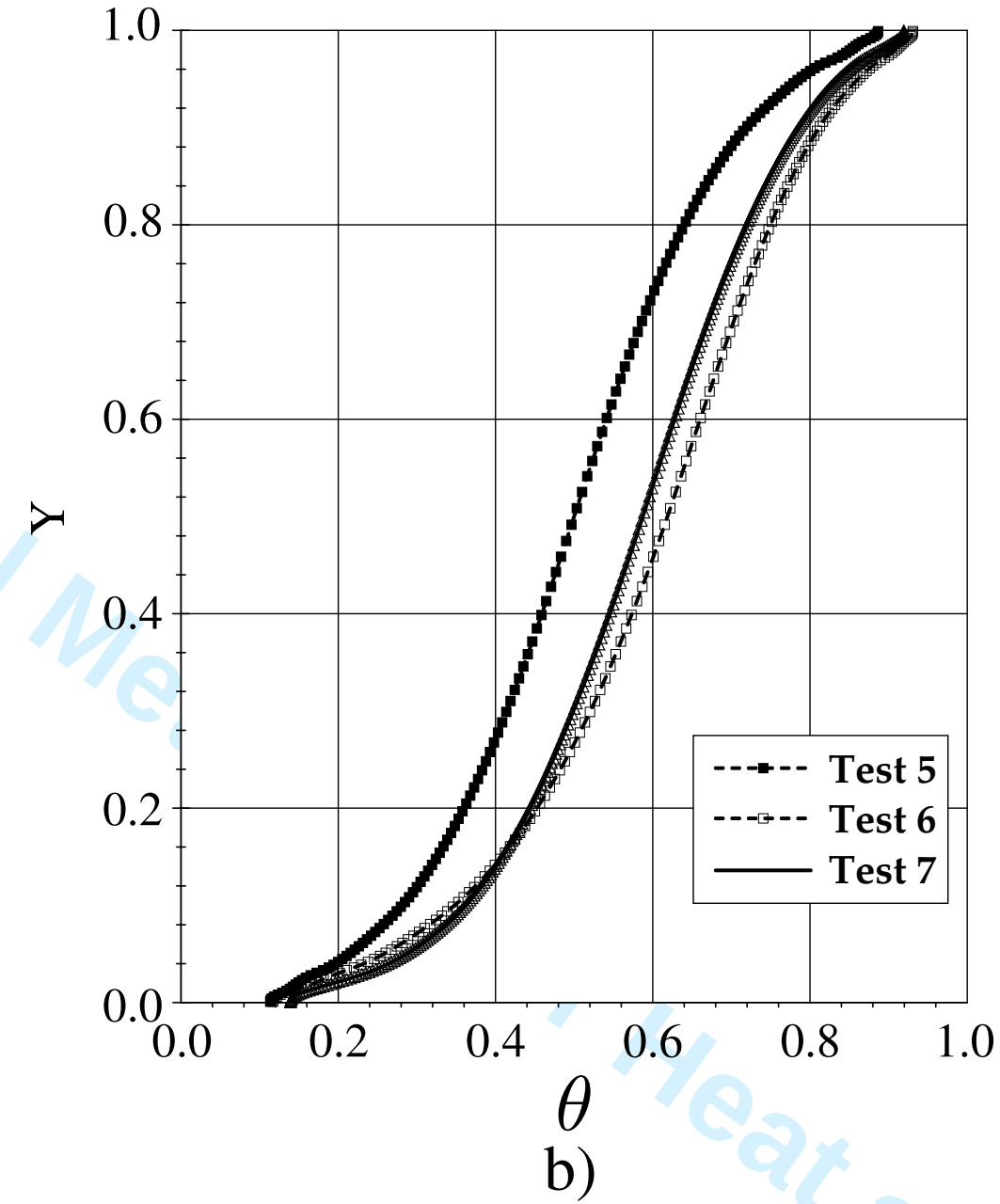
1.0
0.8
0.6
0.4
0.2
0.0
Y
0.0
0.2
0.4
0.6
0.8
1.0
θ
Test 5
Test 6
Test 7

b)

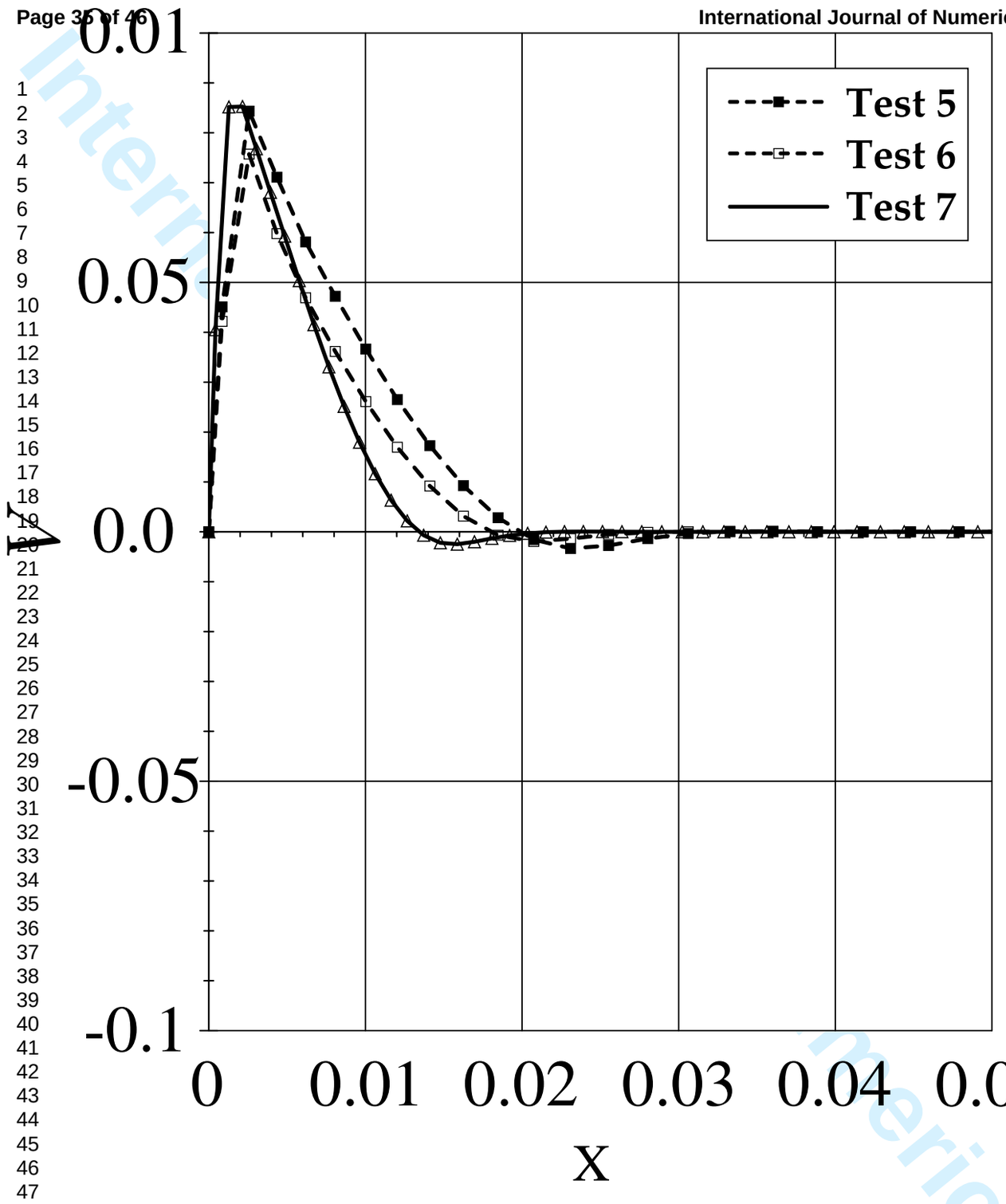
Test 5
Test 6
Test 7
0.01
0.05
0.0
-0.05
-0.1
0
0.01
0.02
0.03
0.04
0.05
x
a)

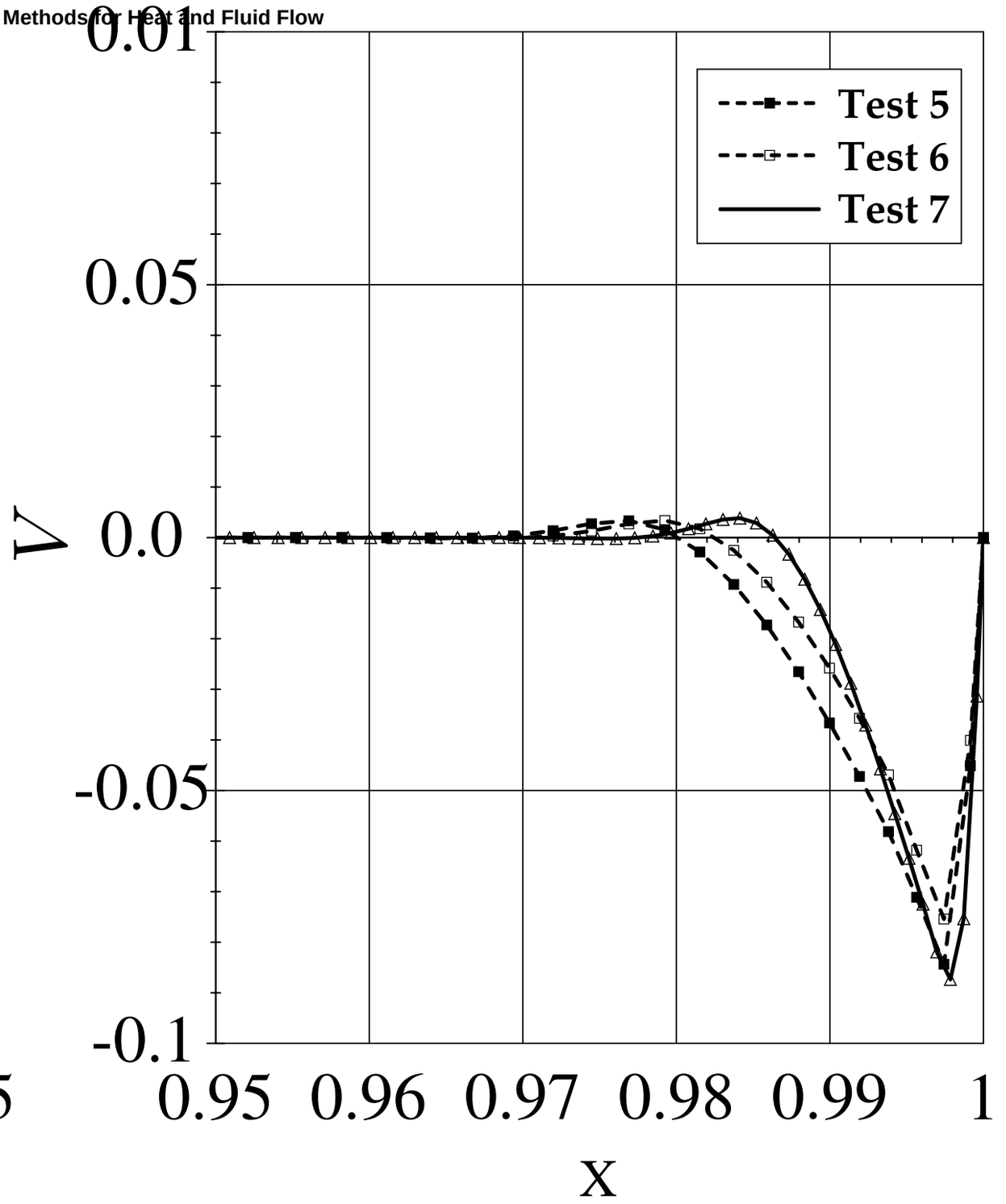
Test 5
Test 6
Test 7
0.01
0.05
0.0
-0.05
-0.1
0.95
0.96
0.97
0.98
0.99
1
x
b)

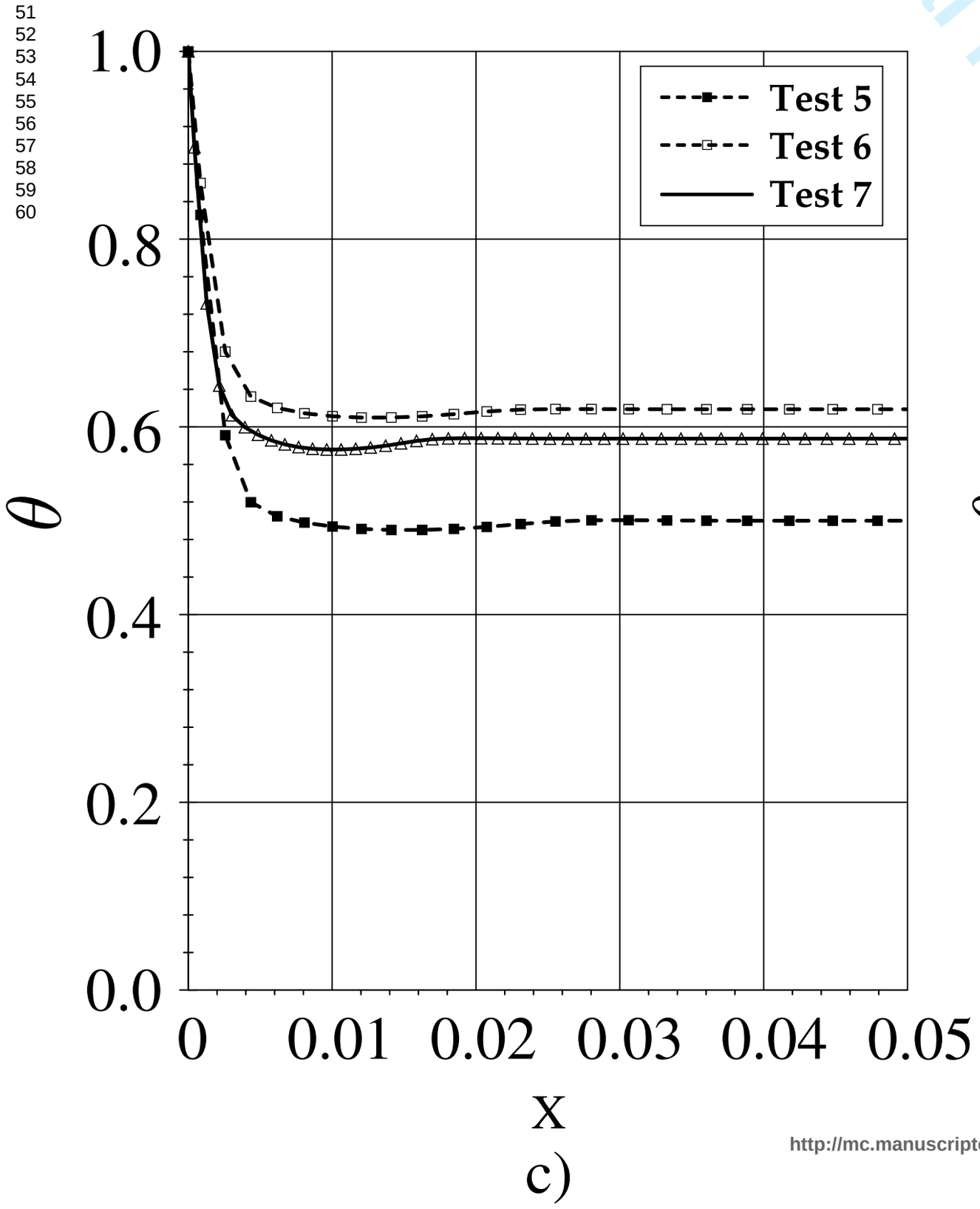
Test 5
Test 6
Test 7
1.0
0.8
0.6
0.4
0.2
0.0
θ
0
0.01
0.02
0.03
0.04
0.05
x
c)

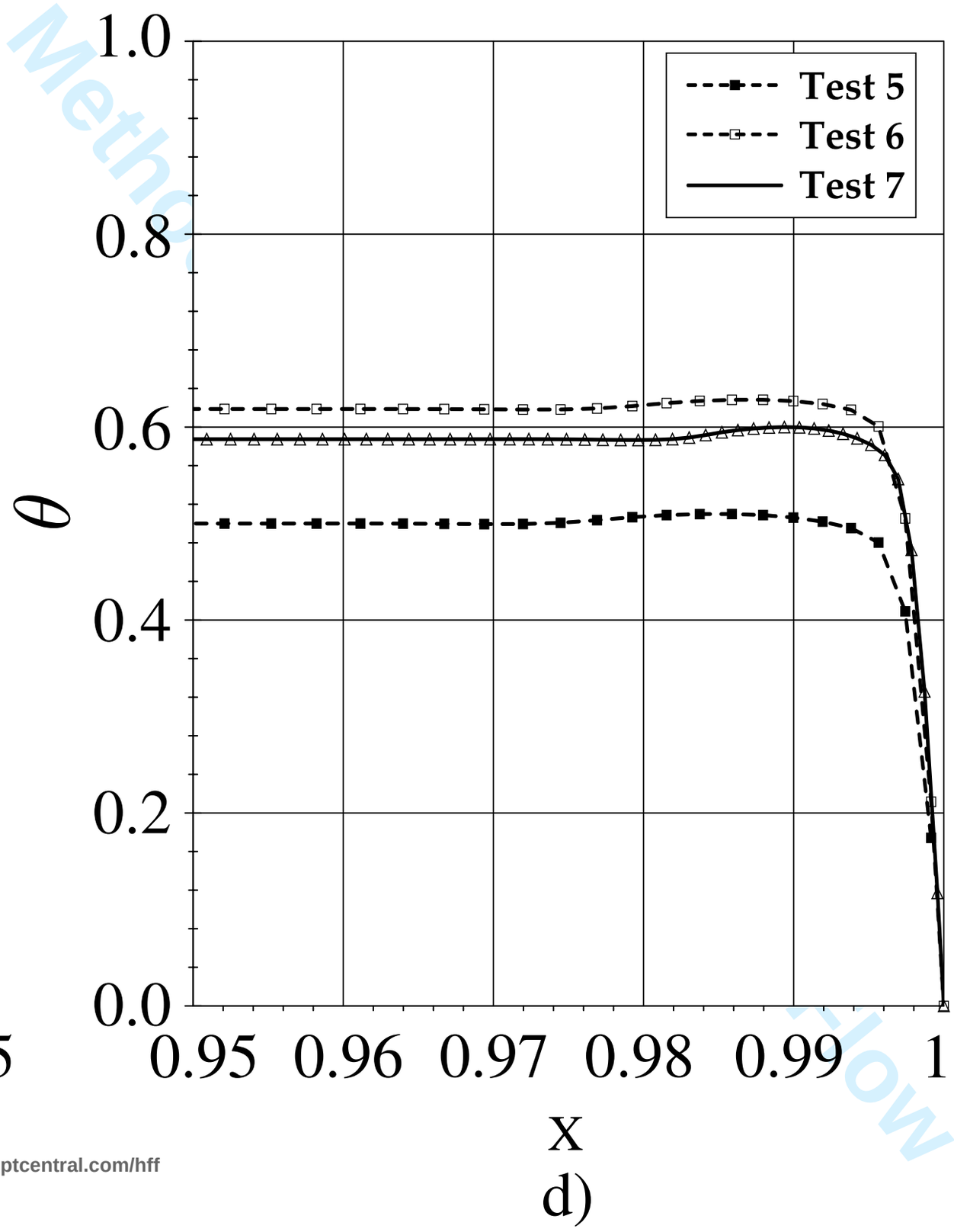
Test 5
Test 6
Test 7
1.0
0.8
0.6
0.4
0.2
0.0
θ
0.95
0.96
0.97
0.98
0.99
1
x
d)

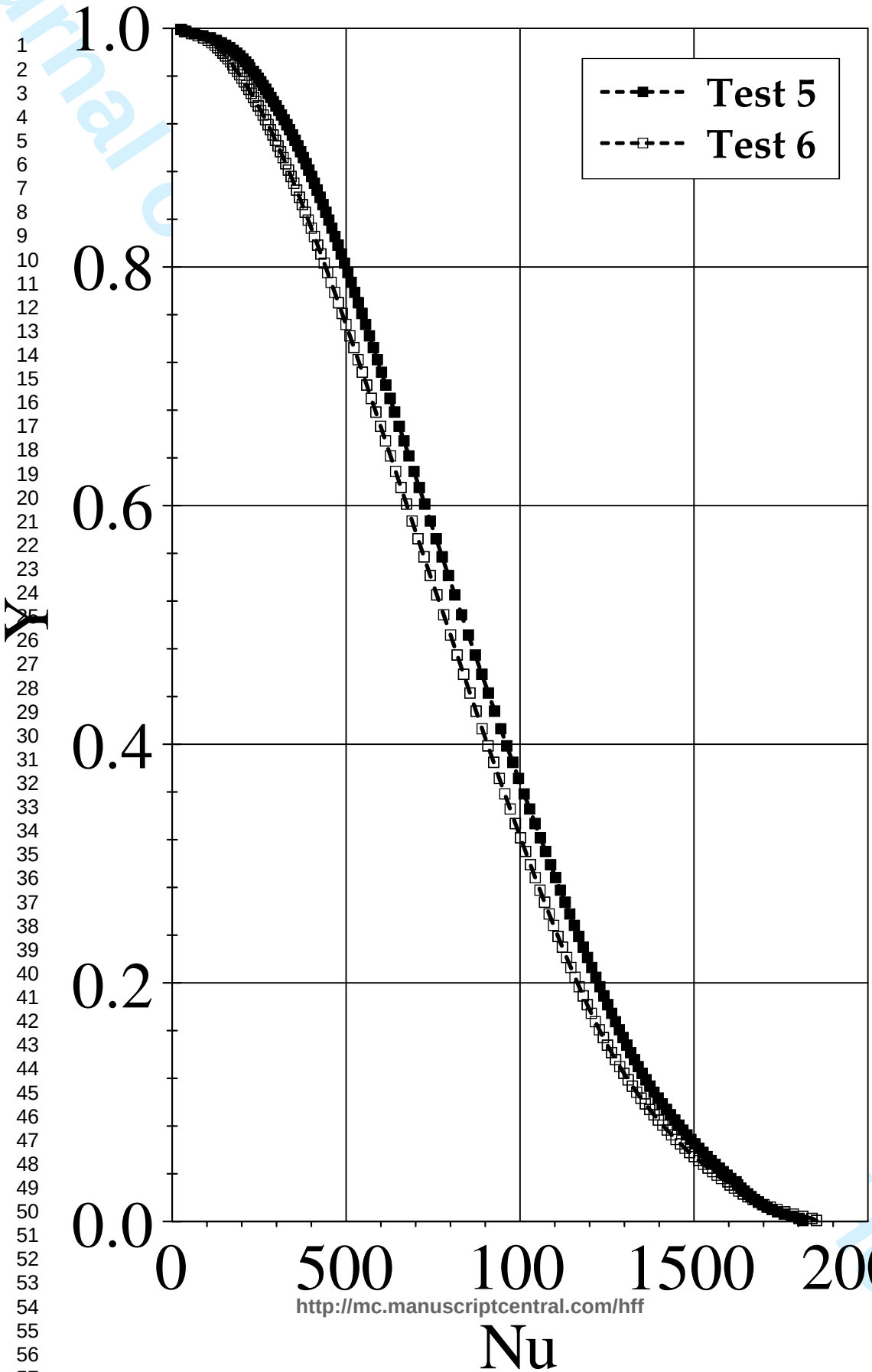
Test 5
Test 6
1.0
0.8
0.6
0.4
0.2
0.0
Y
0
500
100
1500
2000
Nu

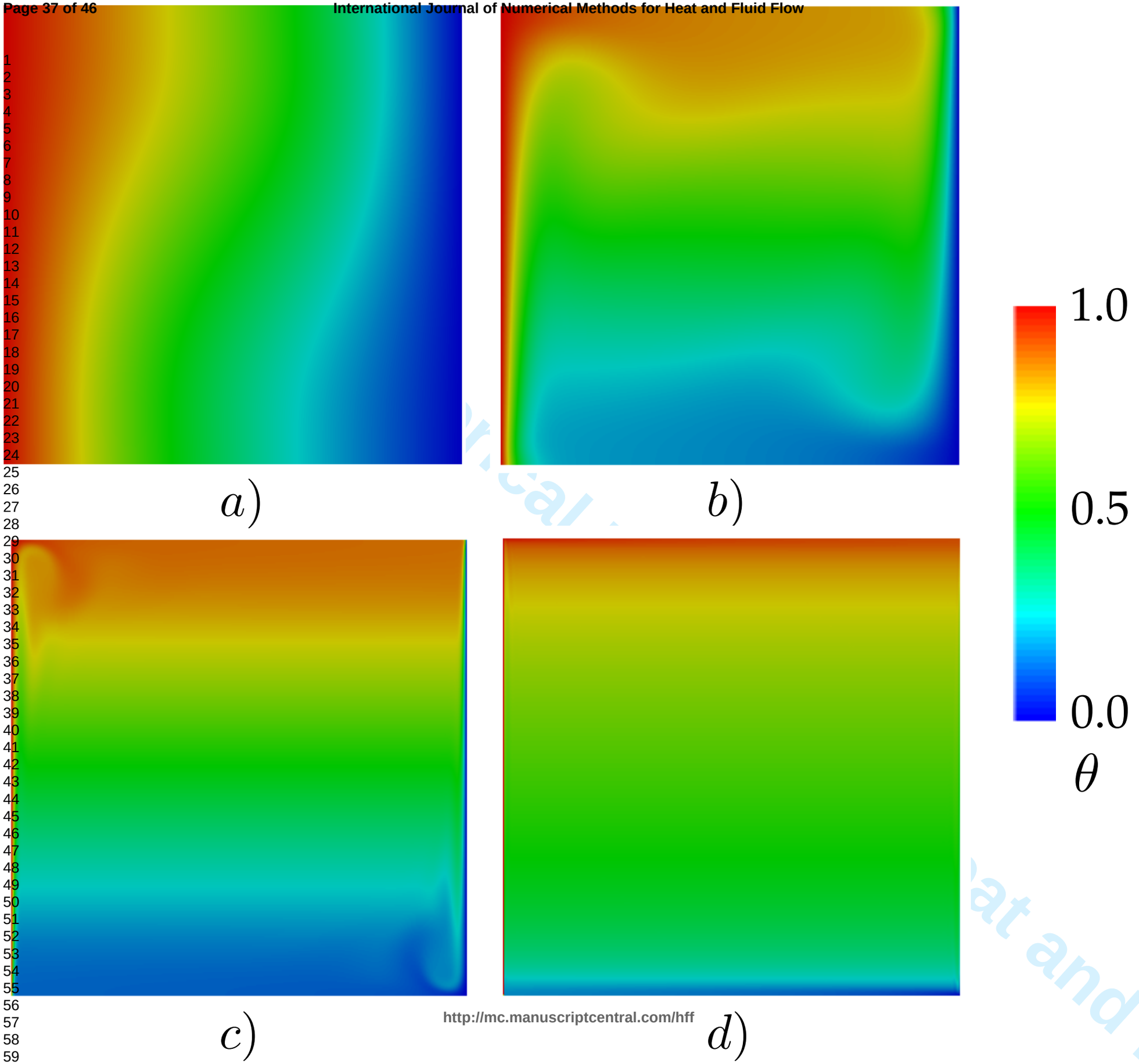
a)
b)
c)
d)
1.0
0.5
0.0
θ

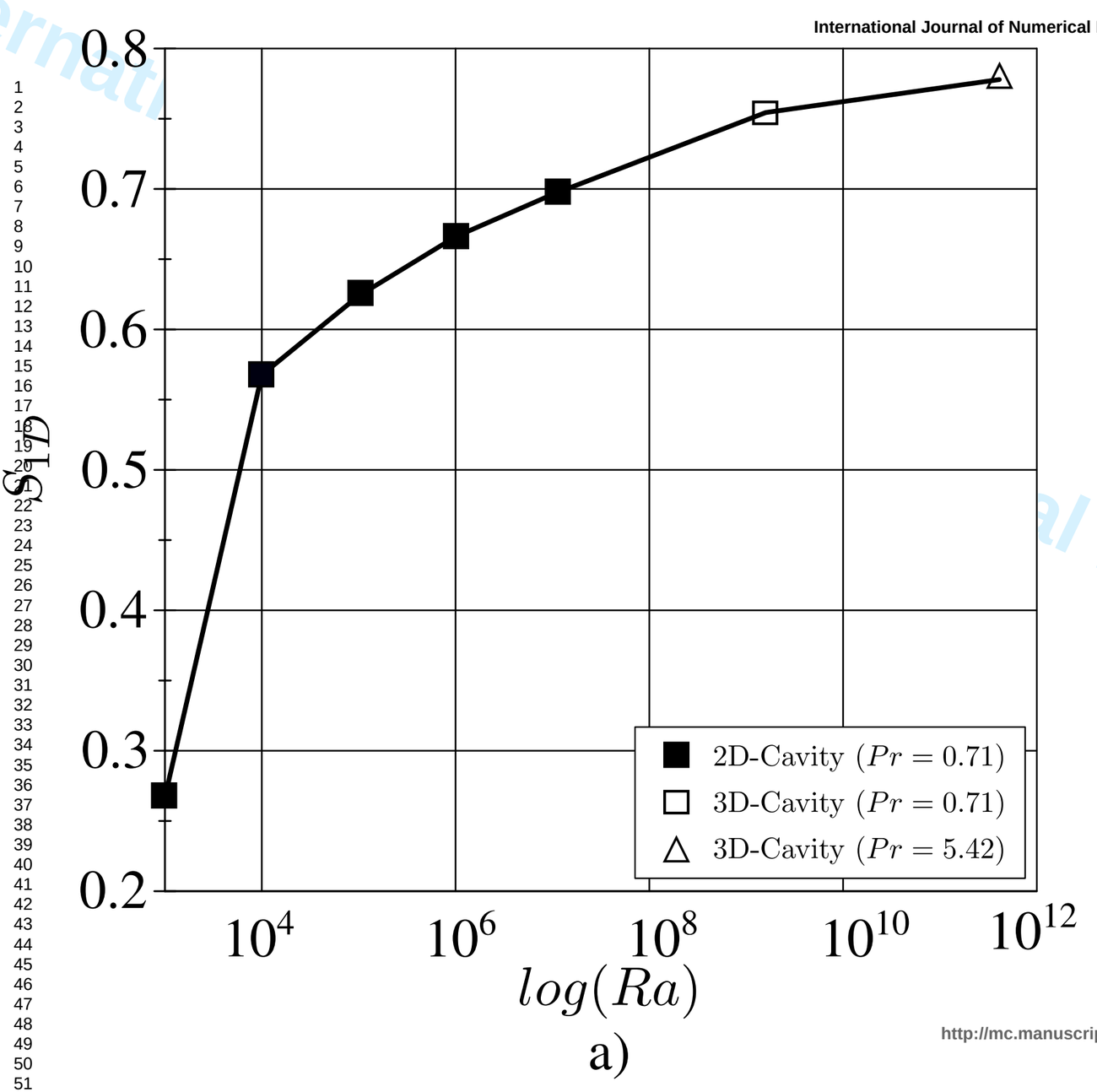
0.8
0.7
0.6
0.5
0.4
0.3
0.2
S_{1D}
10^4
10^6
10^8
10^{10}
10^{12}
$log(Ra)$
2D-Cavity $(Pr = 0.71)$
3D-Cavity $(Pr = 0.71)$
3D-Cavity $(Pr = 5.42)$

a)

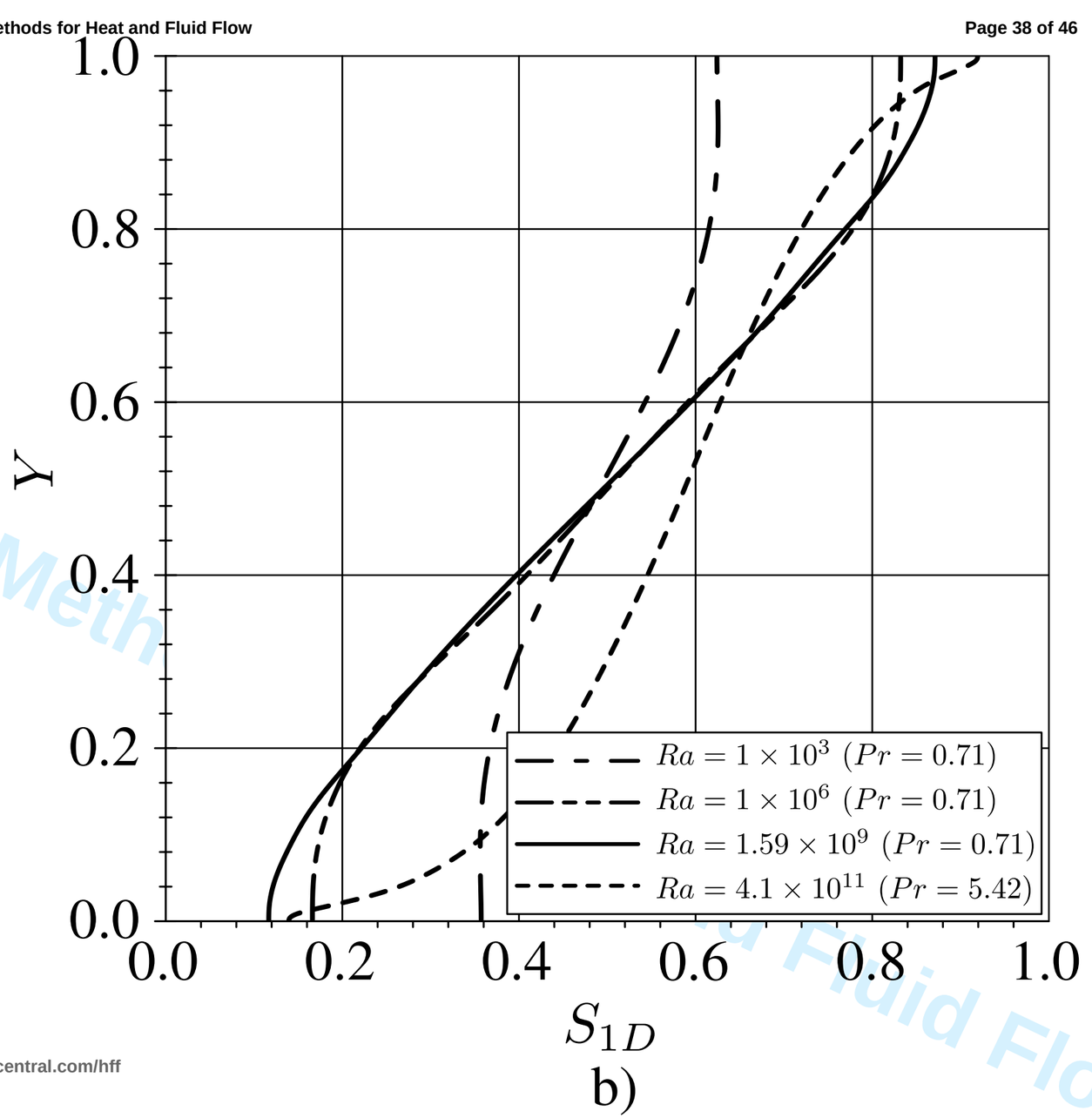
1.0
0.8
0.6
0.4
0.2
0.0
Y
0.0
0.2
0.4
0.6
0.8
1.0
S_{1D}
$Ra = 1 \times 10^3$ $(Pr = 0.71)$
$Ra = 1 \times 10^6$ $(Pr = 0.71)$
$Ra = 1.59 \times 10^9$ $(Pr = 0.71)$
$Ra = 4.1 \times 10^{11}$ $(Pr = 5.42)$

b)

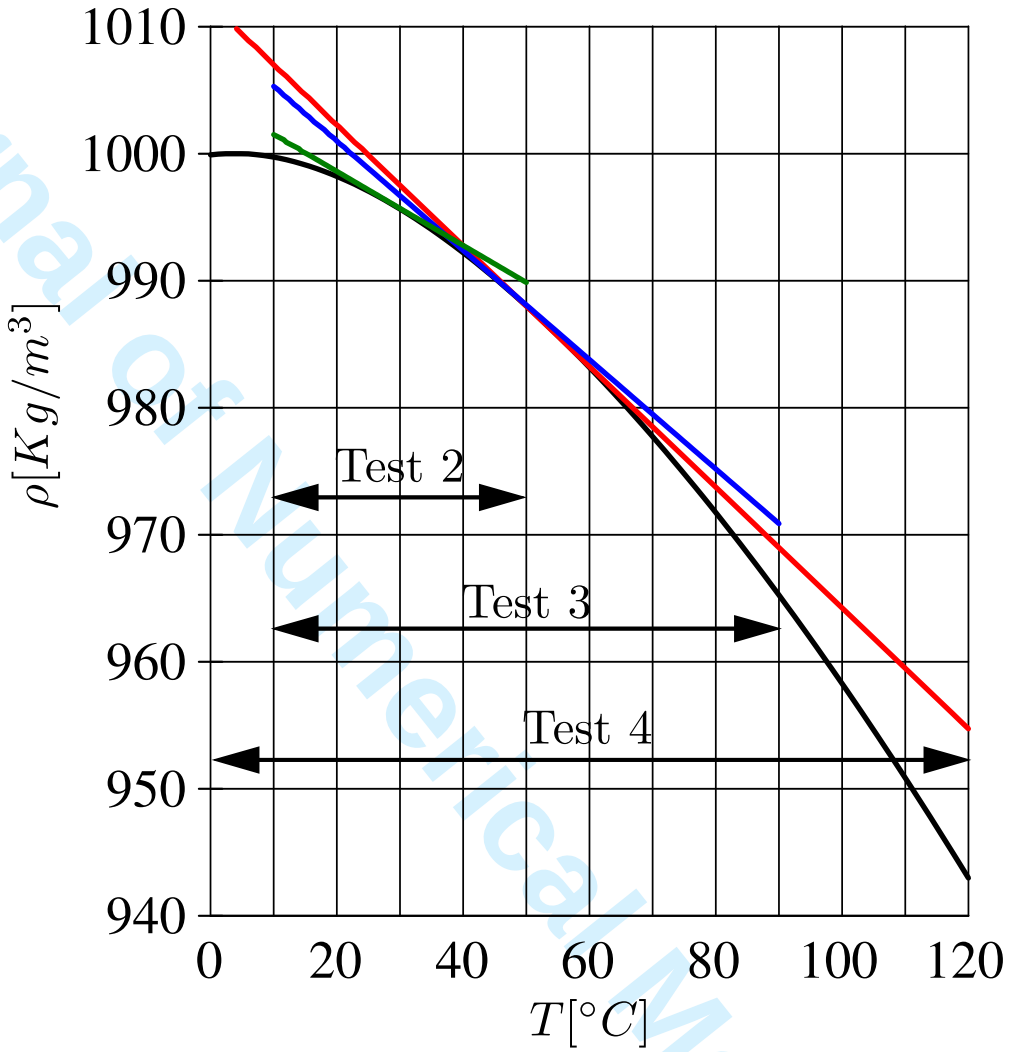
1010
1000
990
980
970
960
950
940
$\rho[Kg/m^3]$
Test 2
Test 3
Test 4
0
20
40
60
80
100
120
$T[°C]$

b)

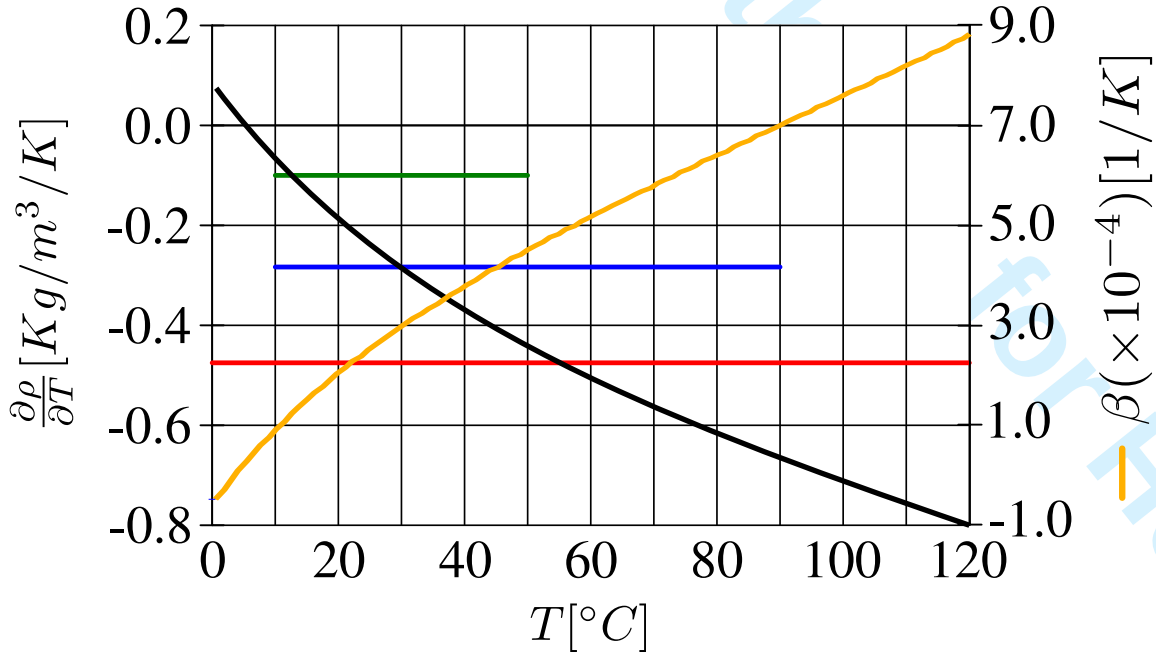
0.2
0.0
-0.2
-0.4
-0.6
-0.8
$\frac{\partial \rho}{\partial T}[Kg/m^3/K]$
9.0
7.0
5.0
3.0
1.0
-1.0
$\beta(\times 10^{-4})[1/K]$
0
20
40
60
80
100
120
$T[°C]$

a)

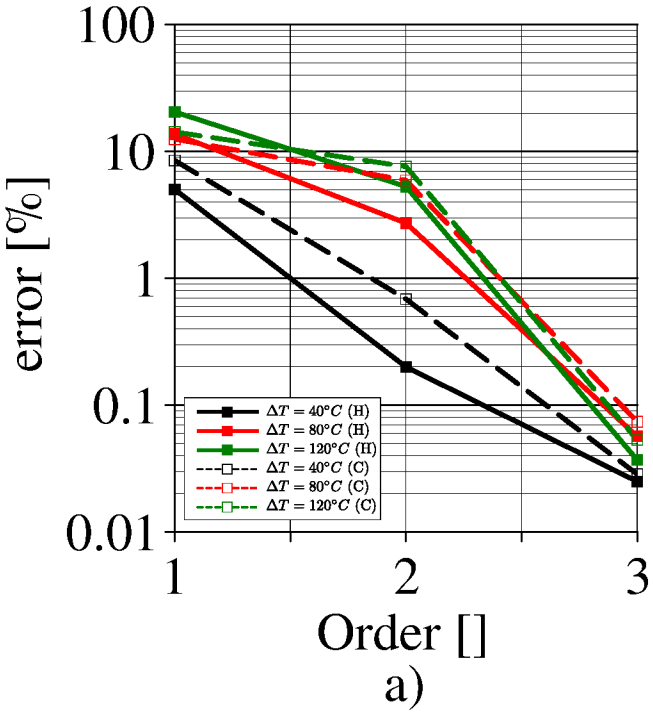
100
10
1
0.1
0.01
error [%]
1
2
3
Order []
ΔT = 40°C (H)
ΔT = 80°C (H)
ΔT = 120°C (H)
ΔT = 40°C (C)
ΔT = 80°C (C)
ΔT = 120°C (C)

a)

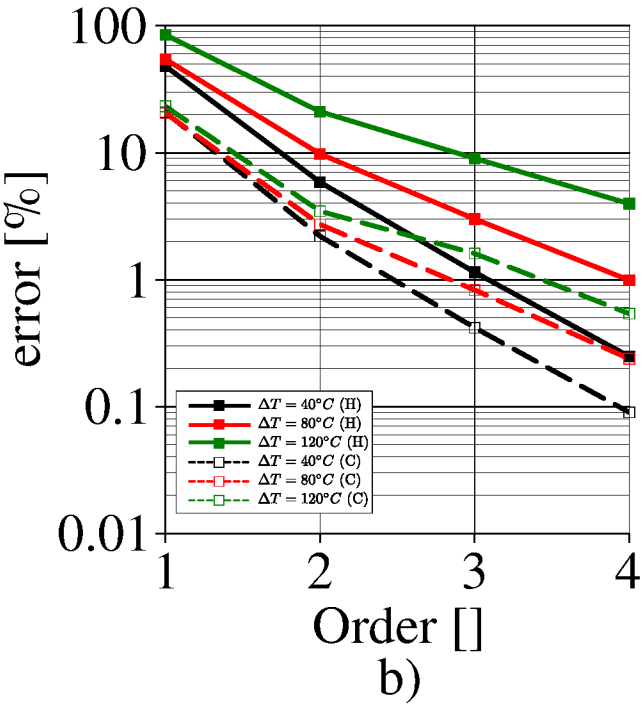
100
10
1
0.1
0.01
error [%]
1
2
3
4
Order []
ΔT = 40°C (H)
ΔT = 80°C (H)
ΔT = 120°C (H)
ΔT = 40°C (C)
ΔT = 80°C (C)
ΔT = 120°C (C)

b)

To the Editor of International Journal of Numerical Methods for Heat and Fluid Flow

Dear Prof. R W Lewis,

In this letter you will find the answer of all the reviewers requests.

Sincerely,
Dr. Santiago Corzo

Referee #1

This paper compares the Boussinesq model with the conservation equation model in different cases where the natural convection is the dominant phenomenon. It is well known that these models have different solutions. The topic is interesting, however, it lacks of focus and quantitative evaluation. Can we get quantitative information from these tests? The paper can be published after answering the below observations but some parts of the paper need to be rewritten to clearly state new results and key research points.

We agree with the reviewer's contribution. In the new version of the manuscript a new criterion for the Boussinesq approach validity is presented. The research contribution is focussed in a novel point of view and especial effort is devoted to justify the importance of this. Every reviewer requests are answered below:

- **Reviewer: A criterium where to apply the Boussinesq and the conservation equation model should be quantified. Many computations can be found in literature about this topics. We already knew that the models give different results but we need to quantify. The sentences such as "therefore, the criterion to apply Boussinesq approach should be tied up to the second derivative of density.." is not enough for publication.**

In accord with the above mentioned, several paragraphs were included in the manuscript.
In the introduction we added a complete description about the state of the art of the Boussinesq acceptance criteria focusing on the contribution of Gray et al. [Gray1976], which introduced the more referenced criterion. Latterly, several contributions showed that this criterion could be enough restrictive [Zhong1985], [barhaghi2006], [barhaghi2007] [pesso2009] [mlaouah1997], [Peng2000].

On the basis of the literature results, a new criterion should be defined for the Boussinesq validity. As it is well known, the Boussinesq approach leads to a perfectly antisymmetric solution for the simplest differentially cavity problem. This is quite correct for low and mean Rayleigh problems. However, in current study, the differences between the compressible and Boussinesq approach were highlighted for high Rayleigh problems. That allows to propose a criterion based on the

acceptance error on the prediction of the average temperature, which is significant different for both solvers.

In the results section this criterion is defined. The figure 1 (fig. 5 in the manuscript) has been recently included into the manuscript and shows the error in the average temperature as a consequence of the use of the Boussinesq approach.

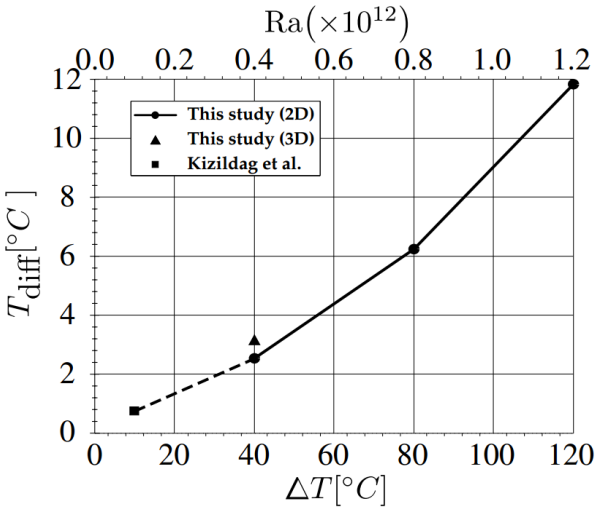

Figure 1. Difference between the average temperature (T_{diff} = T_{avr} - T_{mw}) from the compressible solver and the Boussinesq approach.

As stated above, the differences grow faster than linearly, i.e., for the lower DT (40ºC) the compressible solver estimates a temperature 2.54ºC upper than the expected from Boussinesq; For the medium DT (80ºC) it increases up to 6.24ºC and finally for the larger DT (120ºC) it is 11.81ºC. The relative error increases linearly from around 6.35% for DT=40ºC up to 9.84% for DT=120ºC.

It can be concluded that the error is related more than linearly to the wall temperature range and then to the Rayleigh number. Therefore, it is possible to propose an empirical relationship between the average temperature error and the Ra or the wall temperature range:

$$T_{\mathtt{diff}}(Ra) = 4.93\times10^{-24}Ra^2 + 4.072\times10^{-12}Ra - 0.2331 \quad \text{for} \quad 2.2\times10^{11} < Ra < 1.2\times10^{12} \tag{28}$$

$$T_{\mathtt{diff}}(\Delta T) = 0.000537\Delta T^2 + 0.03042\Delta T + 0.4132 \quad \text{for} \quad 10°C < \Delta T < 120°C \tag{29}$$

Both equations allow estimating the error in the average temperature using Boussinesq approach for a DHC and for water at very high Ra regime. Although the range of validity of these error estimations ($2.2e^{11}$<Ra<$1.2e^{12}$ or 10ºC<DT<120ºC) seems to be small, it is a novel validity criterion to be adopted for a water system subject to industrial conditions. ***The above postulated correlation quantifies the***

mean error and constitutes a valuable contribution to analyze the applicability of the Boussinesq approach.

• Reviewer: The introduction of the LES turbulence model leads to different contributions for the Bousinesq and the conservation equation model. At this point it is not easy to separate the turbulence from the different model contributions. Also 2D turbulence gives a different contribution from 3D turbulence terms. Can we evaluate the different contributions ? Maybe the turbulence should be simply ignored.

It is clear the importance of the turbulent contribution in this type of problems. Several authors have studied the LES contribution for natural convection problems.
In this paper, the main effect of the turbulence model was quantified, showing the reduction on the sub-grid viscosity for the finest mesh. However, a depth analysis of turbulence effects exceed the objectives of this work.
Although the current grids are not enough to perform DNS calculus, as was suggested by the reviewer, we consider that the influence of the turbulence model over the 3D results is small. That is supported by the low eddy viscosity ratio obtained for the finest grids. The follow paragraphs were included in the manuscript to addressed this subject:

In the sub-section **"High Ra problem: air-filled cavity test"**:

> *"Calculations were performed for two meshes:*
> *the coarse mesh was 75x75x40 (with mean y+ = 3.42 and a maximum value of 6.76 in the hot wall) and the finer mesh (named as ref. in graphics) was 150x150x80 (with meany+ = 1.53 and a maximum value of 2.84 in the hot wall). Both grids were locally refined close to the walls. The maximum aspect ratio between the nearest wall cell and the core cells was 10. Despite mesh refinement, it is not enough to neglect turbulence modeling. However, the sub-grid viscosity (mu_{SGS}) is in the same order as the molecular viscosity, thus indicating that the influence of the unresolved scales on the solution is not critical. For this air-filled test mu=1.6267x10^{-5} and the average and maximum mu_{SGS} for the coarse mesh are 6.8190x10^{-7} and 4.35x10^{-5}, respectively. Regarding the finer mesh, the average and maximum values for mu_{SGS} become 1.8586x10^{-7} and 1.66x10^{-5}, respectively".*

In the sub-section **"Very high Ra problem: water-filled cavity test"**:

"... for the 3D cases two meshes were implemented; the coarse one with 150x150x80 hexahedral cells ($1.8x10^6$ cells) and the finer one with 300x300x160 hexahedral cells ($14.4x10^6$ cells) with the same refinement ratio near the walls. Similar than for the previous 3D cases, the sub-grid scale viscosity mu_{SGS} was keep bounded. For example, for the test 1 the molecular viscosity mu was $7.968x10^{-4}$ while the average and maximum mu_{SGS} for the 3D coarse mesh (test 6) were $6.4302x10^{-5}$ and $1.34x10^{-2}$ respectively whereas for the finer mesh (test 7) they become $1.8373x10^{-5}$ and $4.98x10^{-3}$, respectively".

• Reviewer: The solution of the incompressible Boussinesq model by pressure projection, which have different boundary conditions in pressure, can lead to different solutions. Please state clearly the boundary conditions in pressure for the incompressible and for the conservation equation model. Are these boundary conditions the same ? Can we quantify the contribution of these different boundary conditions.

The pressure boundary condition for closure domains need to be defined as a reference value in any cell of the domain. The imposition of a fixed value in each one of the boundary walls could lead to a mistake from the mathematical point of view. On the other hand, a fixed "zero" gradient BC is not correct due to the hydrostatic pressure gradient. For these reasons, the "fixedFluxPressure" BC implemented in OpenFOAM was used. This BC fixes the pressure gradient so that the boundary flux matches the velocity boundary condition when the body forces acts. This BC was the same both for the compressible and the incompressible models.

• Maybe the evaluation of the difference of the two solutions in L^2 the domain could give a better quantitative estimate than the pointwise visual criterium proposed in this paper.

In the current version, we developed an engineering criterion, which allow to quantify the error introduced by the Boussinesq approach. Additionally, in a new subsection at the end of the results section, we discuss some ideas about the accuracy of the density estimation, which can be the initial point in order to improve the Boussinesq approach. We pointed out that a first order approach for the density could be not enough accurate (especially for water) for large temperature range problems. A higher order Boussinesq approach could be a better choice, although the implementation should be investigated.

• Sentences to be clarified or rewritten:

– page 8 section 2.2 line 32 36: the correlation for water density should be written in an explicit way.

All the water properties are calculated from the IAPWS database. That is automatically accomplished by a open access library (https://github.com/romansCode/IAPWS-IF97-OF), which was compilled in OpenFOAM 2.3.1.

Regards the below mentioned grammar mistakes, all these were corrected. The overall new version of the manuscript was revised for an native english person.

– page 8 section 2.2 line 36-37: " ... temperature and pressure simulated"

– page 17 line 52: ".... illustrate the above concluded."

• There are many typos. For examples:

– page 11 line 26: "non slip" − > no slip
– page 12 line 40 "finner" − > finer
– page 12 line 48 "finner" − > finer
– page 12 line 52 "finner" − > finer
– page 13 line 6 "finner" − > finer
– page 13 line 11 "finner" − > finer
– page 17 line 52: ilustrate − > illustrate

Referee #2

It is an excellent piece of work. I suggest its acceptance as it is.

Additional Questions:

1. Originality: Does the paper contain new and significant information adequate to justify publication?: good

2. Relationship to Literature: Does the paper demonstrate an adequate understanding of the relevant literature in the field and cite an appropriate range of literature sources? Is any significant work ignored?: adequate

3. Methodology: Is the paper's argument built on an appropriate base of theory, concepts, or other ideas? Has the research or equivalent intellectual

work on which the paper is based been well designed? Are the methods employed appropriate?: sound

4. Results: Are results presented clearly and analysed appropriately? Do the conclusions adequately tie together the other elements of the paper?: interesting and useful

5. Implications for research, practice and/or society: Does the paper identify clearly any implications for research, practice and/or society? Does the paper bridge the gap between theory and practice? How can the research be used in practice (economic and commercial impact), in teaching, to influence public policy, in research (contributing to the body of knowledge)? What is the impact upon society (influencing public attitudes, affecting quality of life)? Are these implications consistent with the findings and conclusions of the paper?: It clearly contributes to the existing knowledge.

6. Quality of Communication: Does the paper clearly express its case, measured against the technical language of the field and the expected knowledge of the journal's readership? Has attention been paid to the clarity of expression and readability, such as sentence structure, jargon use, acronyms, etc.: ok